2011

Laser texturing of drug eluting stents to improve drug adhesion

Michelle Kay Buehler
Iowa State University

Laser texturing of drug eluting stents to improve drug adhesion

by

Michelle Kay Buehler

A thesis submitted to the graduate faculty

in partial fulfillment of the requirements for the degree of

MASTER OF SCIENCE

Major: Mechanical Engineering

Program of Study Committee:
Pal Molian, Major Professor
Abhijit Chandra
Rohit Trivedi

Iowa State University

Ames, Iowa

2011

TABLE OF CONTENTS

LIST OF TABLES

LIST OF FIGURES

ACKNOWLEDGMENTS

I greatly appreciate the opportunity to work with my major professor, Dr. Pal Molian. He has offered much support, encouragement, and patience throughout my research. His guidance, knowledge, and professional experience were essential to the success of my project.

I also would like to thank my committee members, Dr. Abhijit Chandra and Dr. Rohit Trivedi, for their efforts and contribution to this work.

Thank you to Tyler Steele, Manas Lakshmipathy, Andrew Bean, Robert Mattern Jr. for their technical expertise and training on the Zygo surface profiler. In addition, I would like to thank Dr. Ashraf Bastawros and the Mechanical Engineering Department for the use of their Zygo surface profilers.

Thank you to Dr. Vellareddy Anantharam and Dr. Pallavi Shrivastava for their advice, experience, and help in conducting drug elution studies.

I would like to acknowledge the support provided by the National Science Foundation under the grant IIP-0944979.

Finally, I especially thank my family and husband who have provided the love, support, and encouragement to aid me through difficult times during my graduate career. This thesis is a testament to their success.

ABSTRACT

Drug eluting stents have made significant advances in reducing restenosis over bare metal stents; however, further research is required to decrease the likelihood of late stent thrombosis. Thrombosis is often caused by hypersensitivity to the stent, the polymer, and the drug. This study investigates the potential to eliminate the polymer on drug eluting stents to decrease the chance of the requirement of a second procedure to reopen the artery. Nanosecond laser texturing of metallic stent surfaces generates laser-induced periodic surface structures, also referred to as ripples, which can be utilized to promote drug adherence directly to the stent surface. Surface profilometer results demonstrated that laser texturing significantly improves surface topography over bare metal stents. With a 488% increase in volume per unit area, laser texturing dramatically increased the volume of drug that can be contained in the valleys of the stent surface. In addition, the mean valley slope was improved by 420%, indicating that the aspect ratio of the valleys is significantly higher resulting in a higher resistance to erosion of the drug by the flow of blood during stent placement. Drug elution trials proved that laser texturing of metallic stents offers steadier release rates and better drug adhesion than biodegradable polymer stents. Since drug elution tests are expensive to carry out to determine conditions that will yield the desired release rate, an analysis is made using the weighted property index method and the following surface characteristics: surface area ratio, surface roughness, volume of lubricant per unit area from the bearing ratio analysis, and mean valley slope. This study compared four speeds ranging from 0.5 to 1.25 mm/s and showed that 1.25 mm/s produced the greatest ripple formation while minimizing process time.

CHAPTER 1. GENERAL INTRODUCTION

Introduction

Drug eluting stents have made a substantial improvement towards reducing restenosis when compared to BMS; however, DES are subject to late stent thrombosis (LST) for a much longer period of time than BMS [1]. Thrombosis occurs when a thrombus, breaks away from the wall and is then called an embolus. An embolus can block or significantly reduce blood flow which can lead to a myocardial infarction. DES are more prone to LST than BMS because of multiple factors. The drug's effects that are designed to reduce restenosis also slow the natural healing process [1,2]. Stent malapposition and underexpansion are additional factors [1]. Early removal of antiplatelet therapies can increase the risk of LST [1]. Hypersensitivity to the polymer, drug, or stent induces inflammation [3,4]. Some studies suggest that the polymer is the main factor inducing hypersensitivity [3,5].

This thesis focuses on altering surface texture of the DES so that the polymer carrier can be eliminated. This will reduce hypersensitivity which in turn will decrease the chance that the artery needs to be reopened in a repeat procedure. The polymer carrier not only can cause hypersensitivity, but it can promote thrombus formation or release harmful particulate matter into the blood stream when the stent is expanded [6]. Polymers have been the choice for drug adhesion and elution because their elastic properties provide a higher likelihood of withstanding significant tensile and shear stresses during stent expansion. The polymer must resist flaking and cracking while being immersed in a pulsating flow of blood. If unsuccessful, the polymer could lead to blood clotting [6].

Several studies have been conducted to investigate the potential to eliminate polymer carriers so that the DES is more biocompatible. Polymers chosen have been primarily

nondegradable for the purpose of resisting chemical breakdown that will cause further issues [6]. One alternative is to use a biodegradable polymer [7]. Another alternative that has shown promising results is the use of a titanium-nitride-oxide coating on stainless steel stents [5]. This combines the desired structural properties of stainless steel with the high biocompatibility and corrosion resistance of titanium [5]. An additional potential solution is to use a nano-pourous hydroxyapatite coating which is very biocompatible [8]. It can adhere a drug with a lower concentration directly on top of the coating, or the coating can be mixed with the drug enabling a steady release of a drug with a higher concentration.

Since the primary function of the polymer is to adhere the drug to the stent, we have chosen to alter the surface texture so that the drug can be applied to the stent without the polymer carrier. In this study, we use a nanosecond pulsed laser which can produce small ripples in the surface of the stent and yields a rough texture that will promote adherence of the drug to the surface. The ripples will increase surface area and the volume that the drug can settle into which decreases the likelihood of drug erosion from blood flow during stent placement. These ripples are technically referred to as laser-induced periodic surface structures (LIPSS). Ripples are formed when the surface intensity is near the melting threshold for a given material [9,10]. Wavelength, fluence, and pulse width play important roles in ripple spacing thus affecting the quality of the surface texture [11-13]. Ripple formation is linked to interference between incident waves and waves scattered by particulate and surface topography [10]. Further explanations of the mechanisms that generate ripples are discussed in the “Results and Discussion” section of Chapter 3. There has been much research exploring ripple formation using nanosecond and femtosecond lasers. We have selected a nanosecond laser for this study because these lasers are commercially available

making it more appealing to be implemented in the production of stents. Though femtosecond lasers can produce a higher quality and consistency of ripple structures, they lack the efficiency required to laser texture the stent at a reasonable cost.

Thesis Organization

This thesis is organized in a journal paper format including two papers in chapters 3 and 4. Chapters 1 and 2 provide the motivation and background for the studies in chapters 3 and 4. Chapter 3 discusses an experiment that tests the feasibility of using nanosecond laser texturing to promote drug adhesion to the surface without the aid of a polymer carrier. This includes preliminary studies used to determine experimental settings to texture stent surfaces for the drug elution trial. In addition, surface analysis was performed to compare the surface topography between a laser textured surface and one that was not textured. Surface characteristics include surface area ratio, surface roughness, volume per unit area, and mean valley slope. This trial also included a comparison of elution profiles for four stents treated with different conditions. The first stent did not receive laser treatment or a polymer to adhere the drug to the surface. The second stent received laser treatment but did not receive a polymer. The third stent did not receive laser treatment but was aided by a biodegradable polymer. The last stent received laser treatment and the biodegradable polymer.

The study conducted in chapter 4 was an extension of the surface analysis technique conducted in the study in chapter 3. It was a test designed to determine the feasibility of using surface characteristics to compare samples manufactured under different experimental conditions. The goal of this evaluation method is to determine which parameters are the most likely to improve surface adhesion in order to narrow the number of potential solutions

before investing in expensive drug elution trials. Software and experimental conditions were chosen to reduce error and are explained in detail in the "Methods of Analysis" section. In this study, four different scan rates of the sample were compared to determine which speed had the greatest chance of improving drug adhesion with a reasonable time to process the stent. Chapter 5 includes general conclusions observed in the studies from chapters 3 and 4. Chapter 6 follows with future work extending the studies in chapters 3 and 4 to different laser beam intensity profiles thus resulting in a greater potential of ripple coverage per pulse decreasing the time required to process the stent.

References

1. Joner, M., Finn, A.V., Farb, A., Mont, E.K., Kolodgie, F.D., and Ladich, E., 2006, "Pathology of drug-eluting stents in humans: delayed healing and late thrombotic risk," J. Am. Coll. Cardiol., **48**(1), pp. 193–202.
2. Daemen, J., and Serruys, P., 2007, "Drug-Eluting Stent Update 2007: Part II: Unsettled Issues," Circulation, **116**(8), pp. 316–328.
3. Virmani, R., Guagliumi, G., Farb, A., Musumeci, G., Grieco, N., and Motta, T., 2004, "Localized hypersensitivity and late coronary thrombosis secondary to a sirolimus-eluting stent: should we be cautious?," Circulation, **109**(6), pp. 701–705.
4. Nebeker , J.R., Virmani, R., Bennett, C.L., Hoffman, J.M., Samore, M.H., and Alvarez, J., 2006, "Hypersensitivity cases associated with drug-eluting coronary stents: a review of available cases from the Research on Adverse Drug Events and Reports (RADAR) project," J. Am. Coll. Cardiol., **47**(1), pp. 175–181.

5. Windecker, S., Simon, R., Lins, M., Klauss, V., Eberli, F.R., and Roffi, M., 2005, "Randomized comparison of a titanium-nitride-oxide-coated stent with a stainless steel stent for coronary revascularization: the TiNOX trial," Circulation, **111**(20), pp. 2617–2622.
6. Hunter, W., 2006, "Drug-eluting stents: Beyond the hyperbole," Advanced Drug Delivery Reviews, **58**(3), pp. 347–349.
7. van der Giessen, W.J., Lincoff, A.M., Schwartz, R.S., van Beusekom, H.M., Serruys, P.W., and Holmes, D.R.,1996, "Marked inflammatory sequelae to implantation of biodegradable and nonbiodegradable polymers in porcine coronary arteries," Circulation, **94**(7), pp. 1690–1697.
8. Rajtar, A., Kaluza, G., Yang, Q., Hakimi, D., Liu, D., Tsui, M., Lien, M., Smith, D., Clubb Jr, F.J., and Troczynski, T., 2006, "Hydroxyapatite-coated cardiovascular stents," EuroIntervention, **2**(1), pp. 113–115.
9. Guosheng, Z., Fauchet, P., and Siegman, A., 1982, "Growth of spontaneous periodic surface structures on solids during laser illumination," Phys. Rev. B., **26**(10), pp. 5366–5381.
10. Jee, Y., Becker, M.F., and Walser, R.M., 1988, "Laser-induced damage on single-crystal metal surfaces," J. Opt. Soc. Am., **5**(3), pp. 648–659.
11. Yasumaru, N., Miyazaki, K., and Kiuchi, J., 2003, "Femtosecond-laser-induced nanostructure formed on hard thin films of TiN and DLC," Appl. Phys. A., **76**(6), pp. 983–985.

12. Yasumaru, N., Miyazaki, K., and Kiuchi, J., 2005, "Fluence dependence of femtosecond-laser-induced nanostructure formed on TiN and CrN," Appl. Phys. A., **81**(5), pp. 933–937.

13. Jost, D., Luthy, W., Weber, H., and Saiathe, R., 1986, "Laser pulse width dependent surface ripples on silicon," Appl. Phys. Lett., **49**(11), pp.625–627.

CHAPTER 2. BACKGROUND

Background

Coronary artery disease (CAD) is the number one killer of both men and women in the United States [1,2]. It is responsible for 500,000 deaths and 1.2 million myocardial infractions (heart attacks) annually [2]. CAD is the hardening and accumulation of plaque in arteries reducing the diameter through which blood can flow [1]. Patients who have CAD experience a variety of symptoms [1]. Reduced blood flow will cause angina (a pain in the arms, chest, and lower jaw) which can typically be alleviated with rest [1]. This is mild compared to a heart attack when the artery is blocked by a blood clot. If not treated, the heart muscle affected by the clot will turn into scar tissue [1]. Patients with CAD have three main options that are recommended depending upon the severity of the plaque buildup. If CAD is recognized early enough, a patient may manage it by eating a healthier diet and increasing exercise [1]. Other patients may receive an angioplasty, with or without the support of a stent, which is a noninvasive surgery that opens the artery [1]. When the reduction in blood flow is substantial, invasive coronary bypass graft surgery is typically recommended [1,2,3]. This thesis focuses on improving drug eluting stents to decrease the chance of the need to reopen the artery in a second procedure.

Coronary stenting combines a balloon angioplasty and the support of a stent to hold the artery open. The balloon angioplasty opens the artery by expanding a balloon tipped catheter to compress the plaque on the artery wall which in turn opens the targeted area allowing an increase in blood flow [3]. The stent is a wire mesh cut from a hollow metal tube [1,3,4] that is inserted in its compressed state and expanded in the artery with the balloon

catheter. It is used as scaffolding to hold the artery open after the procedure is complete [1,3,4].

While the balloon expansion process compresses the plaque to the walls of the artery, the stress causes damage to the artery wall. This initiates several biological healing responses leading to restenosis. Restenosis occurs with and without a stent; however, it is termed "in-stent restenosis" when a stent is used [3]. Restenosis is caused by elastic recoil, negative remodeling, neointimal proliferation, reorganization of thrombus, and inflammation [2,3,5-9]. The support structure of the bare metal stent (BMS) will prevent elastic recoil and reduce negative remodeling (vascular contraction) [5,6,7]. BMSs have been proven effective by reducing restenosis rates from 30-40% in patients receiving solely a balloon angioplasty to 15-20% in patients receiving coronary stenting [6]. Since over 80% of percutaneous coronary interventions utilize stents, a solution was required to reduce the other problems caused by balloon angioplasty. A drug was needed that is immunosuppressive, antiproliferative, anti-inflammatory, antithrombotic, and a prohealing agent [3,5]. In addition, a method was necessary to apply the drug in a high enough concentration to be effective without causing systemic toxicity.

Drug eluting stents (DES) became the solution to prevent restenosis. DES combine the scaffolding necessary to support the artery after balloon angioplasty with a drug vehicle to deliver the drug directly to the artery wall right after the artery is damaged [3,4,6]. This is particularly advantageous because DES can deliver drug concentrations necessary to be effective while not causing systemic toxicity [3,4,6]. Drugs designed to prevent restenosis are combined with polymers in various methods to attach the drug to the stent and elude it at a

constant rate over a long period of time [3,4]. Common methods of elution include diffusion, dissolution or degradation of the polymer, osmotic pressure, and ion exchange [4].

References

1. Michaels, A.D., and Chatterjee K., 2002, "Angioplasty versus bypass surgery for coronary artery disease," Circulation, **106**(23), pp. E187–E190.
2. Hunter, W., 2006, "Drug-eluting stents: Beyond the hyperbole," Advanced Drug Delivery Reviews, **58**(3), pp. 347–349.
3. Burt, H. M., and Hunter, W.L., 2006, "Drug-eluting stents: A multidisciplinary success story," Advanced Drug Delivery Reviews, **58**(3), pp. 350–357.
4. Acharya, G., and Park, K., 2006, "Mechanisms of controlled drug release from drug-eluting stents," Advanced Drug Delivery Reviews, **58**(3), pp. 387–401.
5. Van der Hoeven, B., Pires, N., Warda, H., Oemrawsingh, P., van Vlijmen, B., Quax, P., Schalij, M., van der Wall, E., and Jukema, J., 2005, "Drug-eluting stents: results, promises and problems," International Journal of Cardiology, **99**(1), pp. 9–17.
6. Waksman, R., 2002, "Drug-eluting stents: From bench to bed," Cardiovascular Radiation Medicine, **3**(3–4), pp. 226–241.
7. Costa, M.A., and Simon, D.I., 2005, "Molecular basis of restenosis and drug eluting stents," Circulation **111**, pp. 2257–2273.
8. Daemen, J., and Serruys, P., 2007, "Drug-Eluting Stent Update 2007: Part II: Unsettled Issues," Circulation, **116**(8), pp. 316–328.
9. Fattori, R., and Piva, T., 2003, "Drug eluting stents in vascular intervention," The Lancet, **361**(9353), pp. 247–249.

CHAPTER 3. NANOSECOND LASER INDUCED PERIODIC SURFACE STRUCTURES ON DRUG ELUTION PROFILES IN STENTS

A paper to be accepted by *The ASME Journal of Medical Devices*

Michelle K. Buehler[1,2] and Pal A. Molian[1,3]

Abstract

Drug-eluting stents (DES) have profoundly affected the field of interventional cardiology as a transformative technology by dramatically reducing the problem of in-stent restenosis. However, the development of adverse, late stent thrombosis raises the question on the safety profile of DES. Thrombosis is believed to be caused by a combination of several factors including the use of synthetic polymers and their biocompatibility, rapid depletion of the drug, and patient compliance issues related to the anti-platelet therapy. In this paper, we report nanosecond pulsed laser texturing of Nitinol platform stent surfaces and its effects on the drug elution profile and potential elimination of the polymer carrier. Results showed that laser-induced periodic surface structures, also known as ripples, have been generated with spacing from sub-wavelength to super-wavelength. The surface texture parameters – volume of lubricant per unit area and mean valley slope – measured through an optical profilometer were increased by over 4 times suggesting that the ripples would serve as effective reservoirs for the drugs. In-vitro drug elution studies of the sirolimus drug with and without a polymer for seven days indicated that ripple structures reduced the cumulative sirolimus release from

[1] Graduate student and Professor, respectively, Laboratory for Lasers, MEMS and Nanotechnology, Department of Mechanical Engineering, Iowa State University, Ames, IA 50011.
[2] Primary researcher and lead author.
[3] Co-author.

73% to 25% in drug-coated stents and from 93% to 45% in drug/polymer coated stents. The release profile of sirolimus shows the absence of the “initial burst” phase in the laser textured stent signifying that the rapid depletion of the drug is preventable.

Keywords: Cardiovascular devices, Drug/cell deliver systems, Medical device manufacturing

3.1 Introduction

In recent history, no medical device has garnered more attention than bare metal stents (BMS) and drug-eluting stents (DES). The nation’s number one killer, coronary artery disease, affects 13.2 million Americans (causing 1.2 million myocardial infarctions and resulting in 500,000 deaths annually [1]) has been subsided through the use of these stents. Basically, the stents are metallic meshes with interconnected or interwoven members that act as scaffolding supporting the artery [2-5]. These stents are inserted in a collapsed state across a site of arterial blockage and stretched open by inflating an angioplasty balloon. In the case of BMS, neointimal hyperplasia occurs and causes restenosis that becomes a major obstacle to the long-term success of percutaneous coronary intervention. Restenosis is a complex biological cascade created by vessel wall stretching during angioplasty, disruption of the atherosclerotic plaque, and trauma to the vessel wall caused by the balloon and the stent struts [4]. The pathophysiology of restenosis is characterized by platelet adherence and aggregation, acute inflammatory response, foreign body response, smooth muscle cell migration and proliferation, extracellular matrix synthesis, angiogenesis, and vascular remodeling [6-8]. In-stent restenosis rates are typically reported to occur in 15–20% of patients receiving a BMS for the treatment of simple coronary lesions, but may occur in 30–

60% of patients with complex lesions [6]. In contrast, DES reduced the risk of re-blockage to fewer than 5% of patients and was proven to be much more effective than BMS for lowering the rates of major adverse cardiac events.

Although dramatic improvements have been noted in early restenosis rates in DES over BMS, concerns have been raised on late stent thrombosis (LST) that is chiefly driven by inherently thrombogenic polymer coatings and their biocompatibility; rapid depletion of the drug; and patient compliance issues related to the necessary oral anti-platelet therapy such as Plavix and aspirin. For example, there is a significant increase in the rate of LST for the two FDA-approved and widely used stents (CYPHER and TAXUS), beginning about 12 months after implantation. Data on the potentially fatal LST have spurred many research and development activities in DES that include novel or non-polymer coatings; a bioabsorbable polymeric platform; a new drug (less cytostatic or cytotoxic); innovative techniques of elution (reservoir, dual elution); revised stent design for challenging target bifurcations; and different pharmacologic strategies (e.g. non-polymeric reservoirs, dual drug elution with antithrombotic and anti-inflammatory agents).

We believe that the resistance of DES to LST can be substantially increased by eliminating the polymers, while slowing down the release of the drug and improving the drug storage. It is generally difficult to remove the polymer coating as its purpose is to make the drug adhere well to the metallic stent surface. However, the polymeric carrier liberates potentially harmful particulate matter into the coronary blood stream. In addition, it contributes to delayed healing and hypersensitivity reaction in some cases [9-12]. There are other limitations associated with polymeric coatings such as adhesion, mechanical properties, inflammatory properties, and material biocompatibility. For example, radial expansion of a

coronary stent substantially disrupts the polymer carrier during deformation of the stent structure. Adhesion related failures (e.g., coating lift, undercutting, holes, particulate formation, etc.) can adversely affect the drug release rate. The use of biocompatible polymer coatings with controlled drug release (used in the second generation Endeavor ZES) or bioabsorbable coating minimize some problems of polymer coating. The alternative is to completely eliminate the polymer. For example, a titanium–nitric oxide alloy coating has been applied to stainless steel stents with encouraging results, including decreased platelet adhesion and neointimal hyperplasia compared with BMS [13]. A nanoporous hydroxyapetite (a biocompatible crystalline derivative of calcium phosphate) coating, which can be impregnated with anti-restenotic drugs, is currently under development [14]. Another critical issue is drug storage and its release. The drug can be eluted by one or a combination of several mechanisms: dissolution, desorption of the adsorbed drug, diffusion through the polymer matrix, and polymer degradation and erosion [15]. The ideal release profile would be zero-order for most drugs so that it follows a steady release rate and the drug levels in the body remain constant while the drug is being administered.

In order to test our hypothesis, we consider texturing the surfaces of DES using a nanosecond pulsed laser to generate ripple structures prior to the application of the drug coating. Ripples, also known as laser-induced periodic surface structures (LIPSS), can be effective in storing the drugs as well as assisting in the drug adherence without the need for a polymer. The formation of LIPSS and associated surface texture parameters and their effects on the drug elution profiles were investigated. The proposed novel laser texturing method of DES can result in unique properties that promote tissue healing, improve cell adherence/anchoring and decrease platelet activation and adherence. Such characteristics will

reduce the risks associated with implantation of medical devices, making DES highly versatile and fine pitch. The technology can be extended to other medical devices such as peripheral stents, biliary stents, cerebrovascular stents, vascular grafts, orthopedic fixation devices such as plates and screws, implantable pacing leads and sensors, pacemaker and defibrillator housings, artificial valves, guidewires, catheters, and others.

3.2 Experimental Details

3.2.1 Preparation of Stent

A generic stent pattern was designed based on the state-of-the-art data gathered from the medical device industry on the existing stents. The stent design was then fabricated from a Nitinol (55% Ni, 45% Ti) tube with an initial circumference of 14.68 mm by stretching it to a final circumference of 21.98 mm and then laser cutting (using a pulsed Nd:YAG laser) and electro-polishing to form stents the length of 31.7 mm, with an outer diameter 7 mm and a wall thickness of 0.36 mm. The fabrication/finishing methods along with tolerance specifications and a scanning electron micrograph of a stent are shown in Figure 1.

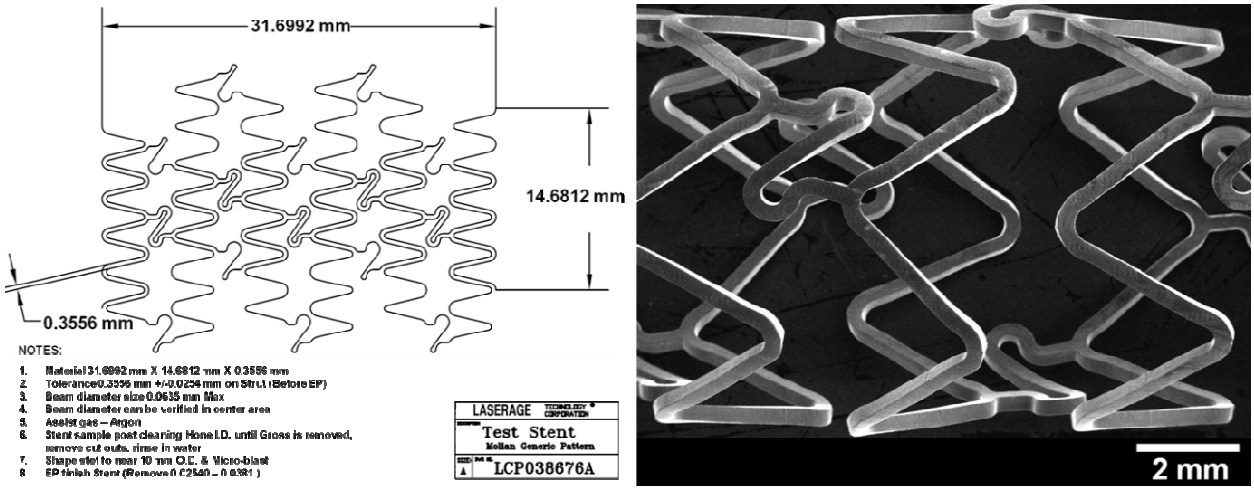

Figure 1: (left) Part drawing and (right) scanning electron image of Nitinol stent

3.2.2 Nanosecond Laser Texturing of the Stent Surfaces

Nanosecond lasers are expected to be highly attractive over femtosecond lasers for texturing because of the lower cost, faster processing, and wider usage in the industry. Prior to texturing the actual stents, small coupons were cut from the stent and then subjected to a 532 nm, 7 ns Q-switched Nd:YAG laser in the direct-writing mode. The coupons with an approximate length of 3 mm, width of 0.36 mm and thickness of 0.36 mm were mounted on an aluminum block using an adhesive tape and then cleaned using methanol to remove any contamination. The aluminum block with Nitinol coupons was mounted on a precision motion, computer-controlled table (X-Y motion). The laser beam was focused onto the coupon surface. A 25 mm diameter, 50 mm focal length spherical lens was used to create a spot diameter of 0.44 mm at the focus. Experiments were performed in an argon gas environment (pressure 68.9 kPa). The process parameters were optimized for a minimum processing time to minimize cost while maintaining an effective texture. The optimum parameters were determined to be pulse energy of 45 mJ, pulse repetition rate of 10 Hz, spot size of 0.44 mm and stent travel speed of 1 mm/s. Figure 2 shows the laser setup and processing of a stent. The stent was mounted on a stainless steel shaft and axially held at the two ends by O-rings as shown in Figure 2b. The beam was transmitted and steered through a set of optics and then focused on the surface of the stent. While the beam was held stationary, a computer motion-controlled linear/rotary platform with an additional provision for automatic rotation in the Z direction was used to move the stent. Four stents have been processed under identical parameters as described above.

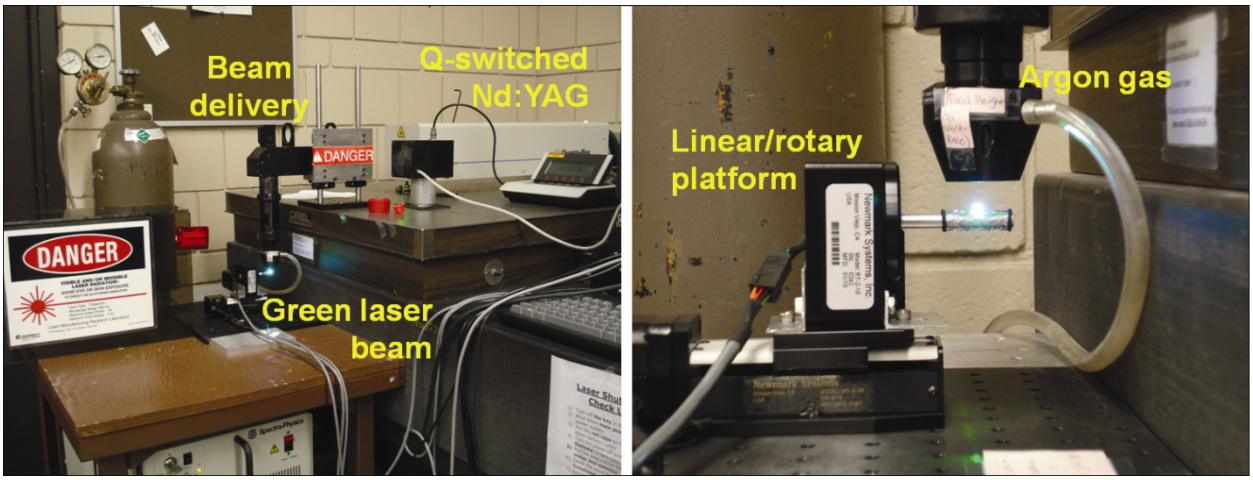

Figure 2: Experimental setup for nanosecond laser nanotexturing of stents

3.2.3 Surface Texture Analysis

Three-dimensional representations of surfaces of four untreated and four laser-textured Nitinol stent coupons were measured and analyzed using the Zygo NewView™ 6000 series optical surface profiler and the associated software, MetroPro 8.3.4. The goal was to obtain the following surface characteristics to determine improvements made by laser texturing: surface area ratio, surface roughness, volume of lubricant per unit area (from the bearing ratio analysis), and the mean valley slope. Height measurements were recorded over a large area that spanned the width of the coupon and a length of 1.44 mm. The large area was necessary because of the fluctuation of the surface topography of the laser-textured coupons. In addition, a 50x objective lens was required to obtain an optical resolution of 0.52 µm. Objectives higher than 50x were not selected because of the substantial amount of data that it would produce rendering it difficult to analyze.

After measurements were recorded, the data was divided in half because of the limitations of computer memory. The form was removed using the “remove curvature” feature. By default, this removes error due to the tilt of the sample. For each section we

recorded the following characteristics: surface area ratio, surface roughness, volume of lubricant per unit area (from the bearing ratio analysis), and the mean valley slope. The surface area ratio is a measure of increased drug adhesion due to the increase in contact area. Surface roughness is a measure of the depth of the indentations in which the drug will settle. The volume of lubricant per unit area is an estimation of the volume of the drug that will lie in the valleys of the surface texture. Finally, the mean valley slope is used to measure the average aspect ratio of the valleys. Each of these characteristics is necessary because no single characteristic can accurately measure the surface texture. For example, surface roughness does not indicate the width of the valleys; however, if the aspect ratio was also taken into account, then we would have a better understanding of the average height and width of the valleys.

Before the results could be recorded it was important to set high and low clips. Data is omitted above a high clip and below a low clip to remove spikes in the data that cause inaccurate results due to the nature of the surface profiler. The high and low clips for the untreated and treated surfaces were ±200 nm and ±1500 nm respectively. Since each coupon needed to be divided in half, a predicted overall value was evaluated for each coupon. The surface area ratio was calculated for each coupon by dividing the sum of the surface areas by the sum of the areas and subtracting 1 to find the increase in surface area due to the texturing process. After the surface area ratio was determined, a high pass Gaussian fast Fourier transform filter with a cut-off wavelength of 11 µm was applied for the remaining surface characteristics. Also, the "trim filter" feature was utilized to decrease error on edges that were caused by the filter. The surface roughness is traditionally calculated as the average of height values; therefore, the halves were combined by averaging the Ra value from each section.

The volumes per unit area were combined by adding the volumes from each half and dividing by the sum of the areas. Lastly, the mean valley ratio was combined by adding the product of the number of valleys and mean valley slope from each section and then dividing by the total number of valleys in the coupon.

3.2.4 Drug Coating Materials

Sirolimus (Rapamycin) was procured from LC Laboratories, Woburn, MA, USA. Rapamycin, a macrocyclic lactone and immuno-suppressive agent, is widely used as a drug for DES because it is known to inhibit proliferation and migration of vascular smooth muscle cells and thereby reducing neointimal formation and restenosis. The polymer used as a drug carrier was a biodegradable type, 50/50 Poly DL lactide-co-glycolide (Purac Inc., USA), also called PLGA, having the inherent viscosity of 1.01 dL/g. The molecular weight is very high on the order of 125,000-150,000 to minimize the polymer erosion. Biodegradable polymers have been extensively used to regulate the drug release rate and also provide the biocompatibility in DES. Among various biodegradable polymers, PLGA copolymers are the most widely applied drug carriers because of their long history of clinical safety. 50/50 PLGA has the fastest rate of degradation in its family, lasting 50 to 60 days. PLGA degrades in the body by simple hydrolysis to non-harmful and non-toxic compounds. The degradation products are either excreted by the kidneys or eliminated as carbon dioxide and water through well-known biochemical pathways. Molecular weight, water uptake, morphological change, and the pH of the release test medium affect the degradation as well as drug release. In addition to the drug and polymer, methanol, acetone, dichloromethane and other chemicals

of HPLC (high performance liquid chromatography) grade were obtained from Sigma Chemical Company, St. Louis, MO.

3.2.5 Drug Coating Procedure

A solution of 2.5% Sirolimus in acetone (25 mg/ml), designated as Solution A, was prepared. The concentration of the drug is comparable with the local tissue concentration of the drug after stent deployment. Solution B was prepared by dissolving 2.5% 50/50 Poly DL lactide-co-glycolide polymer in Solution A. The coatings were applied on both untreated and laser textured stents by a dipping process. All the stents were pre-weighed and dipped in either Solution A or Solution B for 3 min and then dried for 5 min at 50°C in an incubator and weighed. This process cycle was repeated an additional four times.

3.2.6 In-vitro Drug Elution Testing

The coated stents with and without polymer matrix were placed in tubes containing 2 ml of Phosphate Buffered Saline (PBS) of pH 7.4. Then at different predetermined intervals (1, 3, 6, 12, 24, 48, 72, 96, and 168 hrs), the stents were transferred to a new tube containing 2 ml PBS; this gives 8 time point samples per stent. 1 ml was retrieved from the 2 ml PBS for each sample. 800 μL of DCM (dichiloromethane) was added to it and then shaken well for 2 to 3 minutes after which the layers were left to settle down. With the help of a syringe, 3 ml of the fluid was taken out of the vial. A heavy oily lower layer and the watery upper layer were seen. The oily lower layer was extracted and transferred to another vial. The watery layer was again added with DCM, shaken, and the oily layer extracted out of it. This step was repeated 3 to 4 times. Finally when there was only 2 to 3 ml of the oily layer, the vial having

DCM was connected to the rotavapor apparatus to evaporate all the DCM. 200 ml of DCM was added to the residue and transferred to small vials. The vials were opened to the ambient so that DCM could evaporate. 200 µL of methanol was added to the vials and then transferred for HPLC sample trials. Sirolimus standards (0.1-5 µg) dissolved in PBS and extracted with dichlormethane were used as the standards to determine the extraction efficiency of the samples from coated stents.

The rate of sirolimus release was measured using HPLC (Agilent 1100), a system equipped with a Zorbax Eclipse-XDB-C8 column, an auto sampler, and a PDA-UV (photodiode array-ultraviolet) absorbance detector. HPLC analysis was done using a mixture of methanol and 0.1% formic acid in a ratio of 20:80 as a mobile phase with a flow rate of 0.25 mL/min. Column temperature was 37°C, and the injection volume was 10 µl. HPLC was performed in triplicate from a single sample. The peak of sirolimus was characterized using the G135B Agilent-1100 series LC-MS. After running the standard 1 µg for 25 minutes, the online spectrum was taken. The HPLC spectra showed the molecular weight of sirolimus as 914 and the LCMS spectra as 937 (since it combines with sodium, the molecular weight becomes 914+23). This confirms that if a LCMS spectra peak were obtained at 937 molecular weight and 5.2 minutes, the peak is characteristic of sirolimus. The test samples (10 µL each) prepared in methanol were now subjected to HPLC 3 times each and then the chromatograms were extracted from the software. The amount of drug released from DES was calculated after considering the extraction efficiency. The extraction was in the range of 20-30% using a calibration curve with pure sirolimus. The statistical significance of the results was expressed as a p-value which represents the probability of error that is involved in

accepting our observed results as valid. Typically, $p \leq 0.05$ is considered borderline statistically significant while $p \leq 0.005$ is often called "highly" significant.

3.3 Results and Discussion

3.3.1 Nanosecond Laser Texturing

Surface texturing in metals has been reported using nanosecond Nd:YAG and excimer lasers and femtosecond Ti:sapphire lasers [16-29]. Although texturing of metal surfaces can be carried out using various techniques such as grit-blasting, chemical etching, electrochemical etching etc, studies have shown that laser processing offers the benefits of reproducibility and less contamination due to its non-contact nature. This experiment was conducted using a Q-switched Nd:YAG laser in the direct-writing mode. The laser has a wavelength of 532 nm, a pulse width of 7 ns, an average power of 0.45W, and a constant repetition rate of 10 Hz and produces a spot size of 0.44 mm.

In order to determine the location of the ripple pattern created by the nanosecond laser, two laser pulses that directly overlapped each other were targeted on a stent coupon as shown in Figure 3a. Since only two pulses were desired in this case, the repetition rate was slowed to 1 Hz. The results were consistent with another study by Jee et al. in which they investigated damage morphologies with respect to the intensity profile of a Gaussian shaped laser pulse on metal surfaces [30]. It was shown that there are five main zones of damage: boiling, flat melting, ripple patterns, slip lines, and surface cleaning [30]. This is consistent with our findings in Figure 3a. The highest intensity caused the surface to boil creating a crater. Just outside of the center there is a flat smooth section. The ripple patterns are located

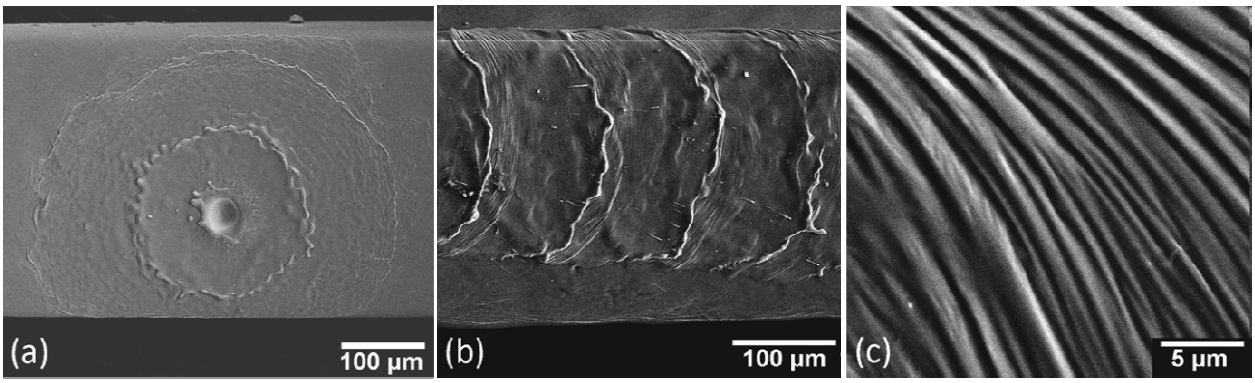

Figure 3: SEM images of nanosecond laser textured coupons: (a) two directly over lapping pulses, (b) overlapping pulses at a speed of 1 mm/s, and (c) closer image of (b) directly outside of the flat melting zone

outside of the flat melting section. The slip lines and surface cleaning sections cannot be observed in the SEM image.

In order to determine what speed to texture the stents used in future experiments, we tested the speeds of 0.5, 1, and 2 mm/s on coupons. The speed of 2 mm/s produced poor ripple coverage; therefore, it was eliminated as a viable option. Figure 3b is an SEM image of the coupon laser treated at 1 mm/s. This option produced quality ripples (Figure 3c) and good coverage directly after the edge of the flat melt zone; however, there is not a consistent coverage in the middle between the edges of the flat melting zones between pulses. Therefore, the speed of 0.5 mm/s was investigated. Though it too produced quality ripples and had better ripple coverage due to the decrease in speed, the same issue arose of inconsistent coverage in the middle between edges of the flat melting zone. After looking at the quality of ripples and coverage area, the lengths of time to create a full sized stent were taken into account because time is a good indicator of cost. The 1 mm/s option required about 30 min to texture an entire stent, and the 0.5 mm/s option required about 60 min. The benefit of better ripple coverage of the 0.5 mm/s option did not outweigh the increased time

to texture; therefore, the speed of 1 mm/s was chosen because it was a compromise between the ripple coverage and minimizing time required to texture the surface.

Figure 4a is an SEM image of the laser textured stent. Figures 4b, c, and d are closer images of areas highlighted in Figure 4a. The main observation is that ripple patterns are finely spaced with periods in the range of 400 nm to 1000 nm. The most prominent texture in Figure 4a is the edge of the flat melting zone from the laser pulse. Since the ripples will be most efficient in securing the drug coating to the stent, the ripples between overlapping pulses were investigated because temperature effects from the previous pulses' higher intensity zones may influence the quality of ripples. Figure 4b and c show that the quality of the ripples was not adversely affected; however, the ripples did not cover the entire area

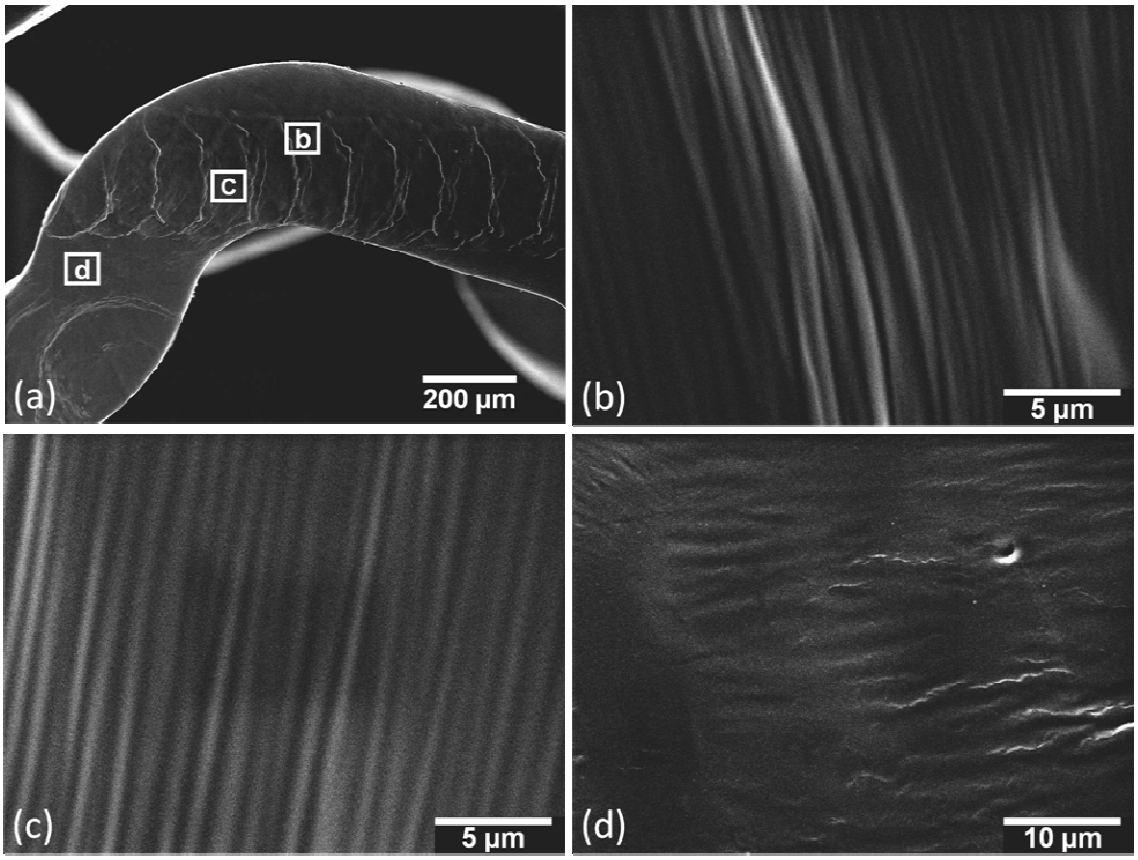

Figure 4: SEM images of nanosecond laser textured stents where images (b), (c), and (d) are closer images of the noted locations in image (a)

which is consistent with the preliminary experiment on the coupon at 1 mm/s. The ripple coverage, as shown in Figure 4d, could be improved between parallel laser paths by reducing the distance between the paths; however, this will increase the time required to texture a stent.

Ripples and associated formation of micro/nanostructures by femtosecond and nanosecond laser irradiation have been studied extensively [16-29]. Siegman et al [16, 17] and Young et al [18, 19] are the first to report a detailed study on laser induced ripples on materials and attributed this to some sort of phase transformation (melting, vaporization, partial, or complete annealing). It was explained that ripples were initiated by the scattering of a small amount of incident light by surface irregularities and subsequent interference between this scattered light and the incident beam to produce a sinusoidal component of spatial variation of light intensity falling on the surface. Each ripple diffracts additional light and a feedback mechanism is then established to create regular periodic ripple structures. Hence, for a normally incident linearly polarized light, the ripples form with crests and troughs running perpendicular to the electromagnetic field direction. The following equation is frequently used to explain the ripple spacing Λ:

$$\Lambda = \lambda/[1 \pm \sin(\theta)] \quad (1)$$

where λ is the laser wavelength and θ is the angle of incidence of the laser on the sample surface.

Typically, the periods of ripples are of the order of incident laser beam wavelength that can be explained by the interference mechanism associated with the inhomogeneities on the material surface. However, ripples have varied spacing in the present work suggesting that mechanisms other than interference become operative. Similar to the present work,

Ozkan et al [20] reported ripples with period 50–100 nm resulting from a 248 nm femtosecond laser irradiation of diamond film. Yasumaru et al [21] observed ripple structures with mean periods of 0.1–0.2 of the laser wavelength. Energy fluence, wavelength and pulse width are the key parameters that influence the periods [21-23]. Besides the interference phenomenon, capillary waves (melting instabilities) [24, 25] or interference of surface plasmons and incident laser radiation [26] are reported to account for the ripple formation. Capillary waves serve as the starting inhomogeneity in the absorptivity of the surface and are responsible for the formation of the initial periodic structure. Shen et al observed circular surface waves when they exposed the Si surface with femtosecond pulses in water [26]. Due to the Gaussian nature of the laser beam, the laser process induces non-uniform heating, generating temperature gradients. The resulting surface tension gradients and the recoil pressure create the hydrodynamic redistribution of the molten region, leading to a breakdown of ripple structures to dimples, pyramids, hills, spikes, spheres, and cones. Thermo-elastically generated surface acoustic waves and micro-bubble formation have also been associated with the formation of ripples [23, 28]. It may be pointed out that femtosecond lasers tend to give rise to cone structures in the nanoscale on the ripples [29].

3.3.2 Surface Topography Analysis

After using the Zygo surface profiler to measure four untreated coupons and four treated coupons, the “remove curvature” feature was applied to measure the surface area ratio. Figures 5a and 6a show examples of the plots after the “remove curvature” feature removed the form from the surface. The red areas indicate peaks, and the blue areas indicate valleys. In order to measure the remaining characteristics, the high pass Gaussian fast Fourier

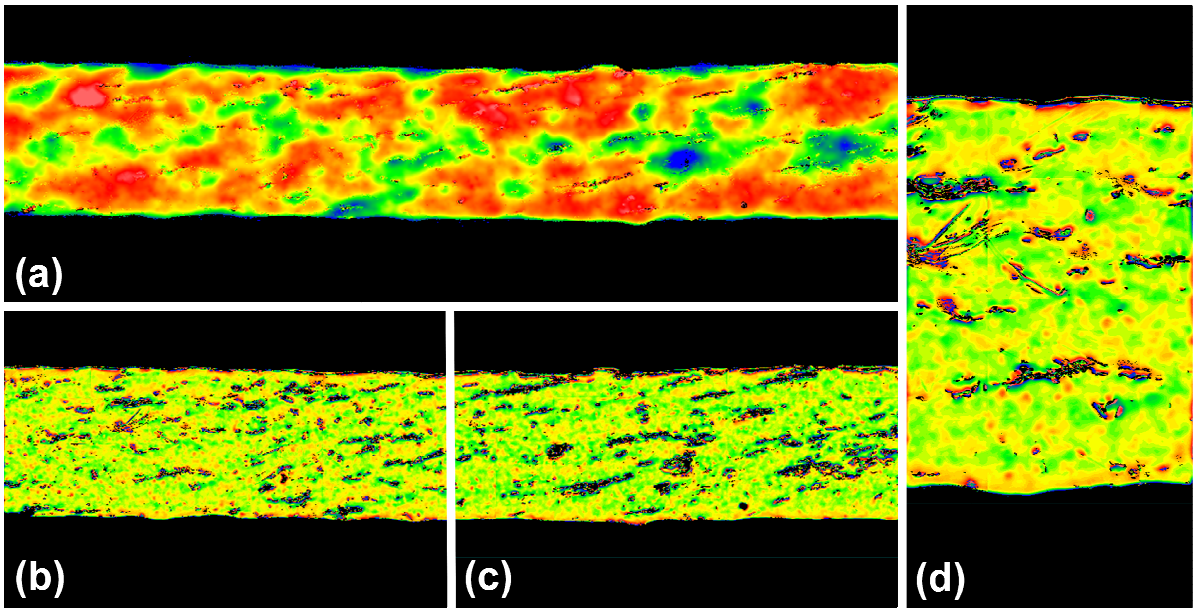

Figure 5: Typical plots from MetroPro of untextured stent coupon where images (b), (c), and (d) are plots after the high pass filter is applied

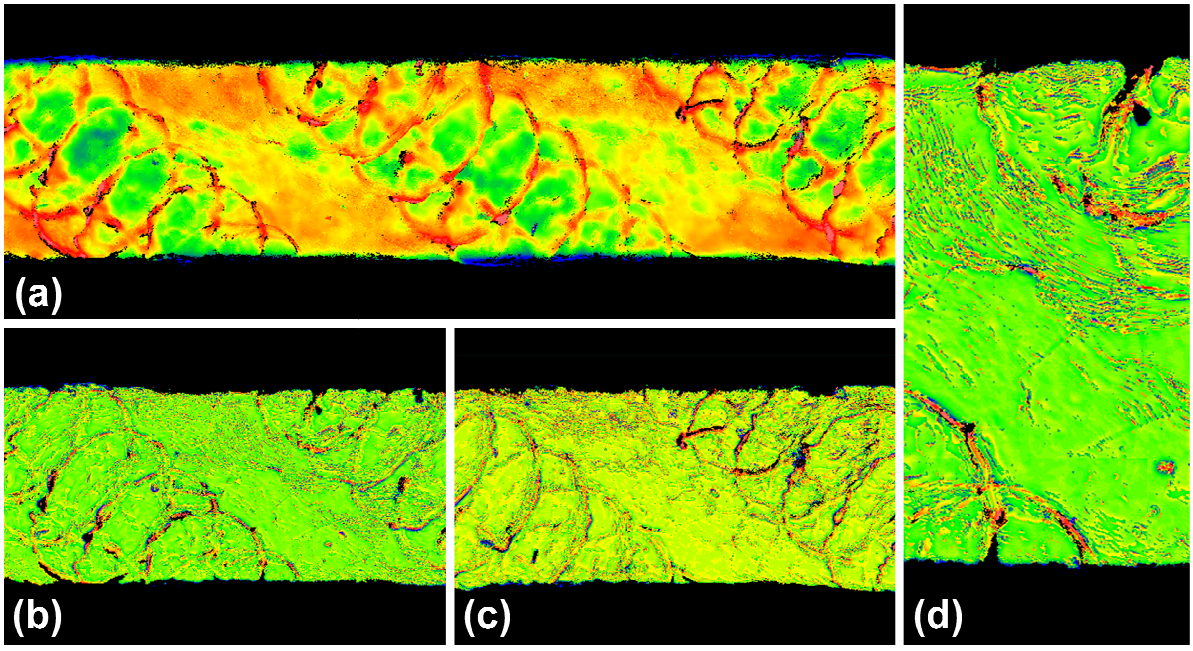

Figure 6: Typical plots from MetroPro of textured stent coupon where images (b), (c), and (d) are plots after the high pass filter is applied

transform filter was applied. Figures 5b, 5c, 6b, and 6c show the left and right halves of the stent coupon with the application of the filter. The majority of the color is green indicating that the filter was effective in removing the form and waviness. The stent was divided into sections due to the limitations of the computer. Figures 5d and 6d are images of a smaller section with a width of one eighth of the length of the measured section. These images show that the filtering process maintains the ripple texture so that the surface roughness, volume of lubricant per unit area, and mean valley slope can be measured after eliminating the waviness of the profile.

Table 1 shows the results of the surface analysis. The percent increase of the mean values of the data sets indicated that there was a significant improvement in surface texture. The 171% increase in surface area ratio shows that the laser texturing process created more contact area on which the drug can bond directly to the surface. The 338% increase in surface roughness was substantial. The texturing process created deeper valleys and higher peaks which is necessary to ensure that the drug will adhere better when the stent is placed. The volume of lubricant per unit area is an estimation of the volume of the drug the stent can hold. The result of an 488% increase from the untreated coupons indicate that the laser texturing method is a potential solution that needed to be further tested in drug elution trials. To ensure that the volume of lubricant per unit area does not simply indicate that the surface

Table 1: Resulting surface characteristics of untreated coupons and treated coupons in addition to their corresponding percent increase due to surface texturing

	Surface Area Ratio [-]		Surface Roughness [µm]		Volume per Unit Area [µm³/mm²]		Mean Valley Slope [µm/mm]	
	Mean	Std Dev	Mean	Std Dev	Mean	Std Dev	Mean	Std Dev
Untreated Coupon	0.095	0.014	0.030	0.004	5860	801	74.1	7.5
Treated Coupon	0.258	0.056	0.131	0.020	34452	3177	385.2	62.4
Percent Increase	171%		338%		488%		420%	

has valleys with low aspect ratios, the mean valley slope was investigated. With an increase of 420%, indeed, the valleys are of a high quality. Since the mean valley slope is a measure of the slope of all valleys including smoother areas as well as areas with a high concentration of ripples, then it is possible to increase the mean valley slope even more by increasing the overlap of parallel paths created by the laser pulses.

Although each of these characteristics will be correlated with each other to some degree, it is important to look at each one. If one of these variables had only a small increase where others had a large increase, then that would indicate that the part of the variable that is not correlated with the other characteristics is what is decreasing the percentage increase. If that was the case, it is possible to determine the cause which could be used to make improvements for future experiments. Since the percentage increases shown in Table 1 are all substantial, this indicates there likely is not a problem.

3.3.3 In-Vitro Release Kinetics

Synthetic or biological polymers are currently used as the matrices for drug incorporation and elution in DES. However there are serious concerns about polymer's biocompatibility and sterility causing inflammation. The deleterious effects of the polymer carrier could be eliminated by directly bonding the drug to the metal platform; however, this method does not allow a large amount of drug to be loaded onto the stent or a slow release of the drug after stent implantation. In this work, we have used the novel laser texturing method to increase the amounts of drug to be loaded while slowing down the drug release rate to the target lesion.

For in-vitro release studies of the drug, four stents were utilized: two from untreated, two from nanosecond laser textured conditions. Two stents, one from each category, were only drug coated while the other two were coated with the drug/polymer. The release kinetics of stents was evaluated using HPLC. Figure 7a shows the characterization of sirolimus by LC-MS/MS (Liquid chromatography-mass spectrometry/mass spectrometry) while Figure 7b shows the sirolimus peak at 5.2 min as detected by HPLC. Figure 8 is the most significant result of our work where the cumulative percentage of drug eluted into the release media is plotted as a function of time. The in-vitro release kinetics for 7 days (168 hrs) at regular intervals for sirolimus only coated stents and sirolimus/PLGA coated stents respectively are shown. The p-values for data sets at each time period are indicated using asterisks in Figure 8. The results are summarized as follows:

1. Nanosecond laser texturing of stent surfaces reduced the sirolimus release rate from 73% to 25% in drug-coated stents and from 93% to 45% in drug/polymer coated stents.
2. Drug/polymer coated stents release the drug faster than the drug-only coated stents; this is attributed to the polymer degradation mechanisms.
3. In untreated stents, 66% and 82% of the drug was released within the 24 hrs in sirolimus alone and in sirolimus/polymer coatings respectively. The release profile of sirolimus shows the characteristic zero order release kinetics for the “initial burst” phase. The early release of the drug is attributed to the dissolution of the sirolimus particles for drug-only coated stents and the rapid bulk erosion of the polymer in drug/polymer coated stents.

4. In contrast to untreated stents, nanosecond laser textured stents coated with sirolimus alone and sirolimus/PDLG released ~16% and ~25% drug respectively within the first 24 hrs. The drug release profiles of laser textured stents do not have the "initial burst" phase suggesting that the drug elution is well controlled. Although the presence of the polymer did not affect the rate of drug release, it increases the amount released. It was observed that release of the drug was due to fluid intake from the simulated biological environment (PBS).

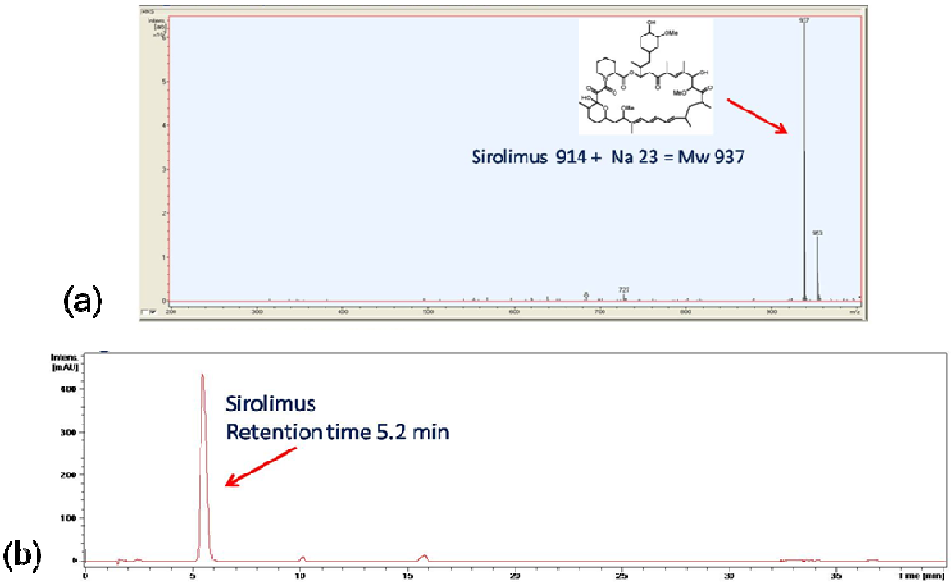

Figure 7: (a) LC-MS/MS characterization of sirolimus; (b) HPLC detection of sirolimus

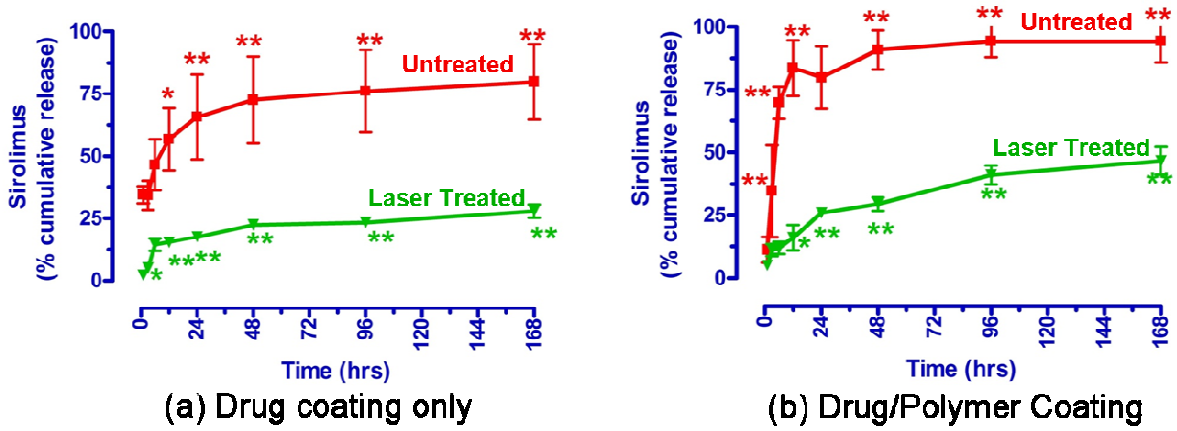

Figure 8: In-vitro release kinetics of sirolimus: (a) with only drug coating; (b) with drug/polymer coating (Statistical analysis: * p< 0.05, ** p< 0.01)

3.3.4 SEM Analysis of Drug Release Mechanisms

SEM studies were conducted on stents after exposure to the release media to observe the changes in surface morphology. All the stents were examined using a FEI Quanta field emission scanning electron microscope (FEI company, Hillsboro, OR, USA). Images were taken of the coating surface from 50X to 1000X magnifications (accelerating voltage of 20 keV). Results are used to determine the distinct drug release mechanisms that are generally classified as dissolution or degradation of the drug or polymer matrix, diffusion of drug molecules, osmosis and ion exchange for ionized drugs.

Figure 9 (with polymer) and Figure 10 (without polymer) show the representative SEM images of untreated and laser-textured stents respectively after seven days of in-vitro testing in PBS. The morphology of the drug-polymer coated surface in the untreated stent reveals many irregularities such as cracking, flaking and delamination (Figure 9a, b). Such features are indicative of polymer swelling followed by building up of osmotic pressure. It is believed that the uptake of water by the polymer matrix might have caused swelling and produced free carboxylic acid groups. PLGA degrades slowly by hydrolysis. Swelling also enables the drug to be released by diffusion through a boundary layer. Thus, the accumulation of polymer degraded debris results in the buildup of osmotic pressure and the breakup of the surface layers through erosion of the coating. The concurrent swelling and erosion of the polymer matrix result in a zero-order release of the drug. Further release pattern is characterized as first order as the rate of drug diffusion out of the swollen matrix is dependent upon the concentration gradient. In contrast to the drug/polymer coated stent, the morphology of drug only-coated surface (Figure 10a, b) consists of only a particulate phase namely the drug. Several regions are devoid of these particles, suggesting that the release of

the drug is via rapid dissolution of the drug particles from the surface in the beginning and then by diffusion without the rate-controlling polymer matrix.

In the laser-textured stents, the polymer degraded and delaminated through some sort of extrusion mechanism (Figure 9c, d). For example, a network of delaminated polymer (Figure 9d) can be seen. Biological degradation of the polymers is thus the primary mechanism causing the drug release. However, the stents with only the drug coating

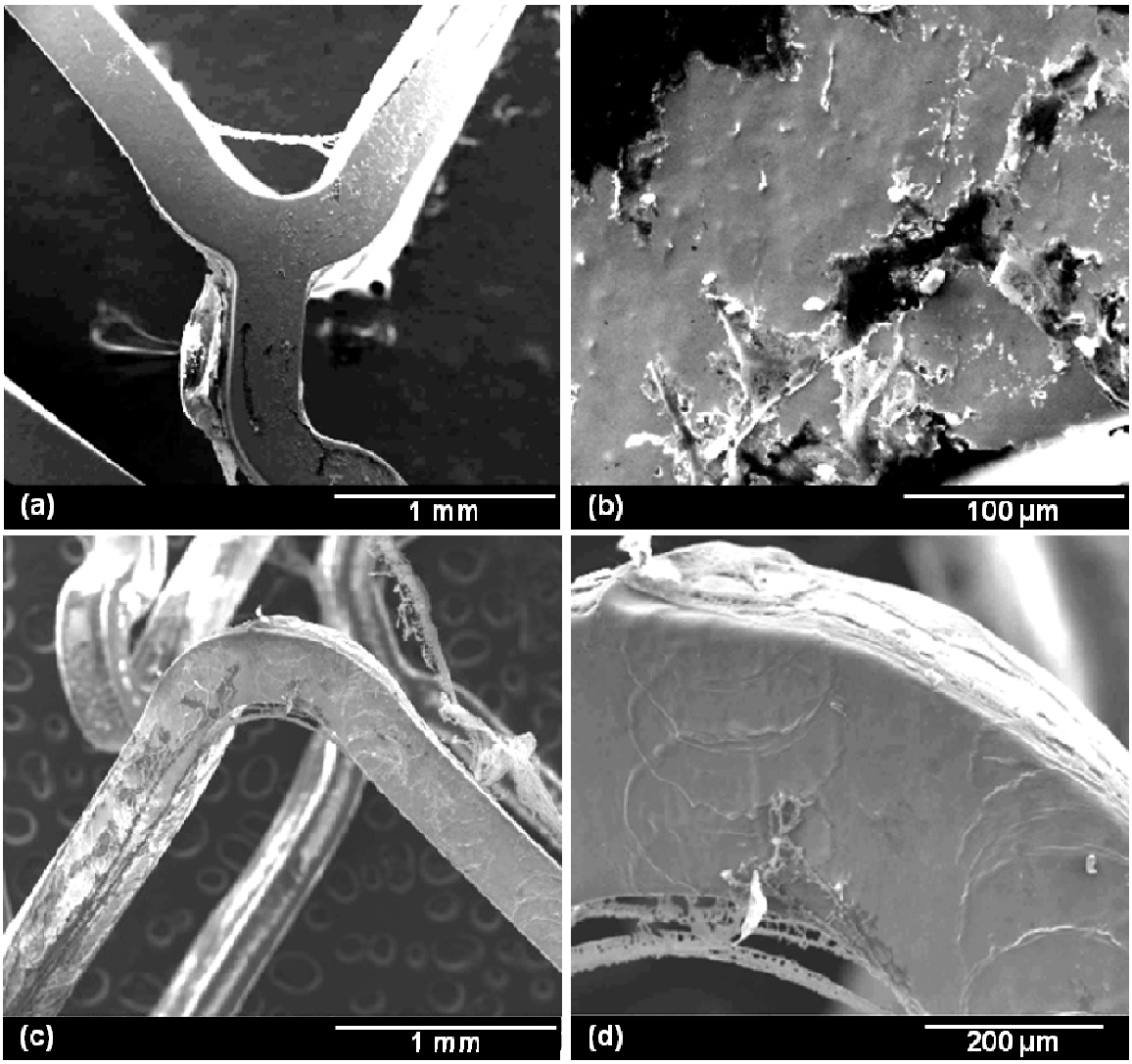

Figure 9: SEM images of stents after 7-days of in-vitro drug release testing. (a, b) Untreated stents: bulk erosion, delamination, osmosis; (c, d) Laser textured stents: delamination of PLGA, drug encapsulation by laser textured scallops

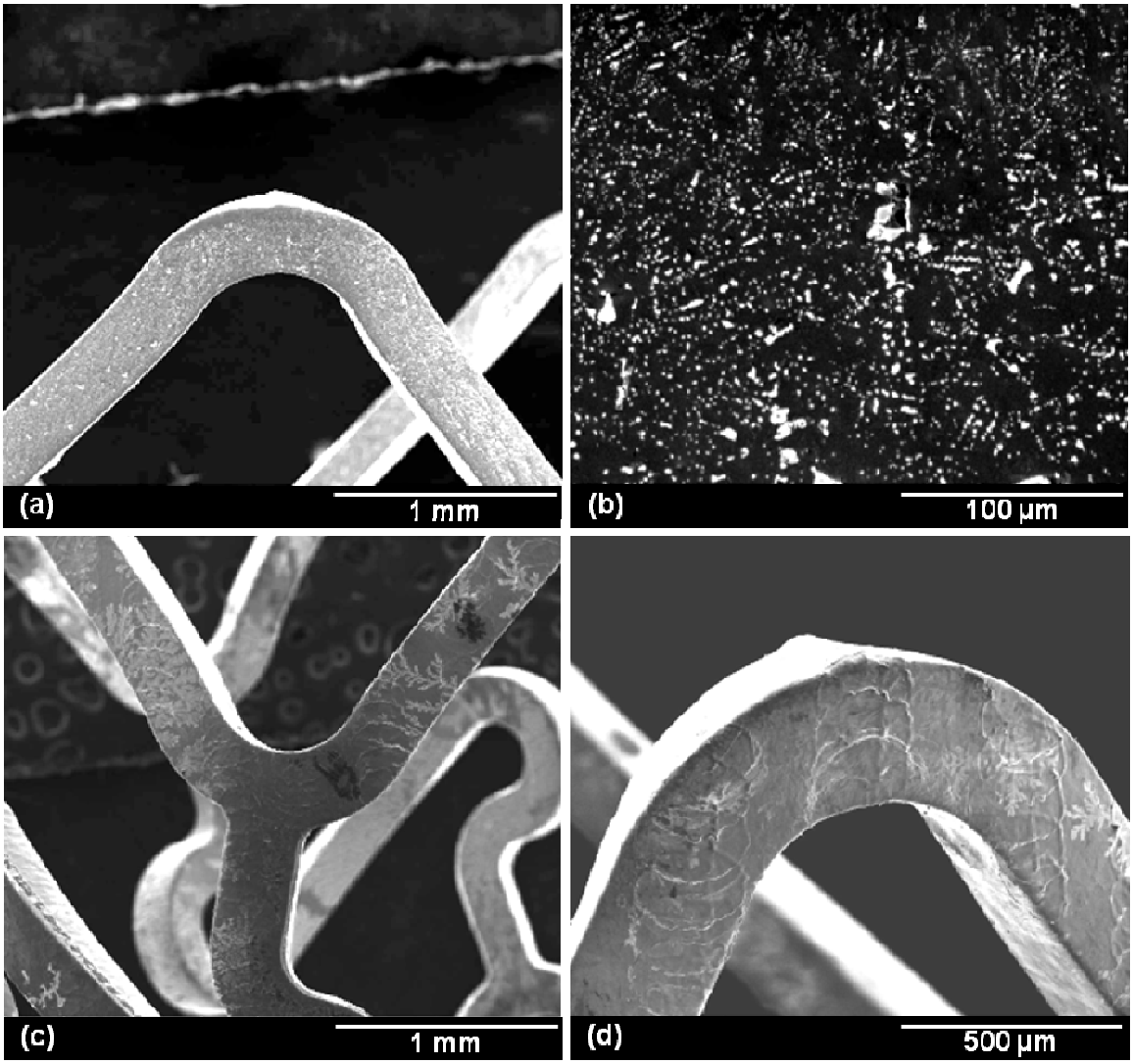

Figure 10: SEM images of stents after 7-days of in-vitro drug release testing. (a, b) Untreated stents: Dissolution/Diffusion of drug; (c, d) Laser textured stents: drug depletion by "tree-like" diffusion patterns

exhibited a tree-like structure of "left over" drugs (Figure 10d). Slow diffusion seems to be the drug release mechanism. In summary, the drug release mechanisms are quite different for those laser textured stents as a result of surface topography and indicate the potential for the utilization of polymer-free drug coatings.

3.4 Conclusions

A Q-switched Nd:YAG laser with a wavelength of 532 nm and pulse width of 7 ns was used to create ripples on the surfaces of Nitinol stents used in interventional cardiology. Following the application of the drug and polymer coatings, the DES was evaluated for drug elution. The principal results and conclusions are as follows:

1. Well organized ripple structures with periods ranging from 400 nm to 1000 nm were obtained.
2. Laser parameters were optimized to facilitate shorter processing time for texturing the stents; this is critical for commercial implementation.
3. Surface topography analysis using an optical surface profiler yielded over a 4 times increase of volume of lubricant per unit area and mean valley slope. This indicated the capability of the surface to retain a significant amount of drug as well as potential for improved adherence when compared to the untreated stents.
4. Drug elution studies confirm that laser nanotextured stents have many advantages over normal stents:
    a. the polymer carrier can be eliminated, because, it did neither contribute to the adherence of the drug nor reduce the drug release rate, suggesting that polymer-free DES can be made possible with laser-textured stents
    b. the rate and percent sirolimus release is significantly lower than untreated stents both in the presence or absence of the polymer carrier. Stents coated with sirolimus/PLDA released 93% and 50% in untreated and nano-laser textured stents respectively over a 7-day period. Similarly, stents coated with the drug alone, released 78% and 25% of sirolimus from untreated and nano-

laser stents respectively over a 7-day period. These results suggest that nano-laser textured stents release sirolimus very slowly (<40%) up to a 7 day period and may extend over 60 days compared to normal stents where >80% is released in the first 4 days.

3.5 Acknowledgements

We like to acknowledge the support provided by National Science Foundation under the grant IIP-0944979.

3.6 Nomenclature

Λ: Ripple spacing

λ: Laser wavelength

θ: Angle of incidence of the laser on the sample surface

3.7 References

1. Hunter, W., 2006, "Drug-eluting stents: Beyond the hyperbole," Advanced Drug Delivery Reviews, **58**(3), pp. 347–349.
2. Daemen, J., and Serruys, P., 2007, "Drug-Eluting Stent Update 2007: Part II: Unsettled Issues," Circulation, **116**(8), pp. 316–328.
3. Burt, H. M., and Hunter, W.L., 2006, "Drug-eluting stents: A multidisciplinary success story," Advanced Drug Delivery Reviews, **58**(3), pp. 350–357.

4. Van der Hoeven, B., Pires, N., Warda, H., Oemrawsingh, P., van Vlijmen, B., Quax, P., Schalij, M., van der Wall, E., and Jukema, J., 2005, "Drug-eluting stents: results, promises and problems," International Journal of Cardiology, **99**(1), pp. 9–17.
5. Waksman, R., 2002, "Drug-eluting stents: From bench to bed," Cardiovascular Radiation Medicine, **3**(3–4), pp. 226–241.
6. Fattori, R., and Piva, T., 2003, "Drug eluting stents in vascular intervention," The Lancet, **361**(9353), pp. 247–249.
7. Costa, M.A., and Simon, D.I., 2005, "Molecular basis of restenosis and drug eluting stents," Circulation **111**, pp. 2257–2273.
8. Chong, P.H., and Cheng, J.W.M., 2004, "Early experiences and clinical implications of drug-eluting stents: part 1," Ann. Pharmacother, **38**(4), pp. 661–669.
9. Joner, M., Finn, A.V., Farb, A., Mont, E.K., Kolodgie, F.D., and Ladich, E., 2006, "Pathology of drug-eluting stents in humans: delayed healing and late thrombotic risk," J. Am. Coll. Cardiol., **48**(1), pp. 193–202.
10. van der Giessen, W.J., Lincoff, A.M., Schwartz, R.S., van Beusekom, H.M., Serruys, P.W., and Holmes, D.R.,1996, "Marked inflammatory sequelae to implantation of biodegradable and nonbiodegradable polymers in porcine coronary arteries," Circulation, **94**(7), pp. 1690–1697.
11. Virmani, R., Guagliumi, G., Farb, A., Musumeci, G., Grieco, N., and Motta, T., 2004, "Localized hypersensitivity and late coronary thrombosis secondary to a sirolimus-eluting stent: should we be cautious?," Circulation, **109**(6), pp. 701–705.
12. Nebeker , J.R., Virmani, R., Bennett, C.L., Hoffman, J.M., Samore, M.H., and Alvarez, J., 2006, "Hypersensitivity cases associated with drug-eluting coronary

stents: a review of available cases from the Research on Adverse Drug Events and Reports (RADAR) project," J. Am. Coll. Cardiol., **47**(1), pp. 175–181.

13. Windecker, S., Simon, R., Lins, M., Klauss, V., Eberli, F.R., and Roffi, M., 2005, "Randomized comparison of a titanium-nitride-oxide-coated stent with a stainless steel stent for coronary revascularization: the TiNOX trial," Circulation, **111**(20), pp. 2617–2622.
14. Rajtar, A., Kaluza, G., Yang, Q., Hakimi, D., Liu, D., Tsui, M., Lien, M., Smith, D., Clubb Jr, F.J., and Troczynski, T., 2006, "Hydroxyapatite-coated cardiovascular stents," EuroIntervention, **2**(1), pp. 113–115.
15. Acharya, G., and Park, K., 2006, "Mechanisms of controlled drug release from drug-eluting stents," Advanced Drug Delivery Reviews, **58**(3), pp. 387–401.
16. Guosheng, Z., Fauchet, P., and Siegman, A., 1982, "Growth of spontaneous periodic surface structures on solids during laser illumination," Phys. Rev. B., **26**(10), pp. 5366–5381.
17. Siegman, A., and Fauchet, P., 1986, "Stimulated wood's anomalies on laser-illuminated surfaces," IEEE J. Quantum Electron, **22**, pp. 1384–1403.
18. Sipe, J.E., Young, J.F., Preston, J.S., and van Driel, H.M., 1983, "Laser induced periodic surface structure. I. Theory," Phys. Rev. B., **27**, pp. 1141–1154.
19. Young, J., Preston, J., van Driel, H., and Sipe, J., 1983, "Laser-induced periodic surface structure. II. Experiments on Ge, Si, Al and brass," Phys. Rev. B., **27**, pp. 1155–1172.

20. Ozkan, A.M., Malshe, A.P., Railkar, T.A., Brown, W.D., Shirk, M.D., and Molian, P.A., 1999, "Femtosecond laser-induced periodic structure writing on diamond crystals and microclusters," Appl. Phys. Lett., **75**(23), pp. 3716–3718.
21. Yasumaru, N., Miyazaki, K., and Kiuchi, J., 2003, "Femtosecond-laser-induced nanostructure formed on hard thin films of TiN and DLC," Appl. Phys. A., **76**(6), pp. 983–985.
22. Yasumaru, N., Miyazaki, K., and Kiuchi, J., 2005, "Fluence dependence of femtosecond-laser-induced nanostructure formed on TiN and CrN," Appl. Phys. A., **81**(5), pp. 933–937.
23. Jost, D., Luthy, W., Weber, H., and Saiathe, R., 1986, "Laser pulse width dependent surface ripples on silicon," Appl. Phys. Lett., **49**(11), pp.625–627.
24. Dolgaev, S.I., Lavrishev, S.V., Lyalin, A.A., Simakin, A.V., Voronov, V.V., and Shafeev, G.A., 2001, "Formation of conical microstructures upon laser evaporation of solids," Appl. Phys. A., **73**(2), pp. 177–181.
25. Shen, M.Y., Crouch, C.H., Carey, J.E., Younkin, R., Mazur, E., Sheehy, M., and Friend, C.M., 2009, "Formation of regular arrays of silicon microspikes by femtosecond laser irradiation through a mask," Appl. Phys. Lett., **82**(11), pp. 1715–1717.
26. Huang, M., Zhao, F., Cheng, Y., Xu, N., and Xu, Z., 2009, "Origin of laser-induced near-subwavelength ripples: interference between surface plasmons and incident laser," ACS Nano, **3**(12), pp. 4062–4070.

27. Shen, M.Y., Crouch, C.H., Carey, J.E., and Mazur, E., 2004, “Femtosecond laser-induced formation of submicrometer spikes on silicon in water,” Appl. Phys. Lett., **85**(22), pp. 5694–5696.

28. Katayama, K., Yonekubo, H., and Sawada, T., 2003, “Formation of ring patterns surrounded by ripples by single-shot laser irradiation with ultrashort pulse width at the solid/liquid interface,” Appl. Phys. Lett., **82**(24), pp. 4244–4246.

29. Nayak, B.K., Gupta, M.C., and Kolasinski, K.W., 2008, “Formation of nano-textured conical microstructures in titanium metal surface by femtosecond laser irradiation,” Appl. Phys. A., **90**(3), pp. 399–402.

30. Jee, Y., Becker, M.F., and Walser, R.M., 1988, “Laser-induced damage on single-crystal metal surfaces,” J. Opt. Soc. Am., **5**(3), pp. 648–659.

CHAPTER 4. SURFACE TOPOGRAPHY CHARACTERISTICS FOR IMPROVING DRUG ADHESION IN LASER TEXTURED STENTS

Modified from a paper to be published in conference proceedings
of The 44th CIRP Conference on Manufacturing Systems June 1-3, 2011

Michelle K. Buehler[4,5] and Pal A. Molian[4,6]

Abstract

Polymer carriers that hold the drug onto drug eluting stents cause late stent thrombosis. Research has been undertaken to eliminate the polymer carrier by applying the drug directly onto a laser textured stent. A Q-switched Nd:YAG laser was used to texture stents with different overlaps. A 3D optical profilometer captured height data that was used to analyze the following surface topography characteristics for each overlap: surface area ratio, surface roughness, volume of lubricant per unit area, and mean valley slope. These characteristics are selected to identify which experimental conditions are most likely to improve drug adhesion to the stent.

4.1 Introduction

Drug eluting stents have been proven to significantly reduce in-stent restenosis [1-3]; however, the polymer carrier that holds the drug causes late stent thrombosis [2,3]. Some trials have been conducted without the polymer by applying the drug directly to the stent. An example is a trial with the Achieve™ stent that was dip-coated in a drug alcohol solution [3].

[4] Graduate student and Professor, respectively, Laboratory for Lasers, MEMS and Nanotechnology, Department of Mechanical Engineering, Iowa State University, Ames, IA 50011.
[5] Primary researcher and lead author.
[6] Co-author.

The main problem with this method is the rapid loss of drug before it is placed which leaves an insufficient amount of drug to be used to reduce restenosis [3]. Similarly, this study was designed to work with bare metal stents; however, the surface texture was altered to increase the likelihood of drug adhesion to the stent. A Q-switched Nd:YAG laser was used to create a microstructured surface consisting of indentations and channels in which, the drug will settle and provide better contact to adhere to the surface.

It has been well established that texturing a smooth surface improves coating adhesion [4-10]. This idea is further supported by Mehilli et al. in a trial that demonstrated that a sand blasted, non-polymer based drug eluting stent is comparable to a non-textured polymer based drug eluting stent with regards to reducing restenosis [11]. Sand blasting was not chosen to be investigated in this study because laser texturing has the advantage of being a non-contact process which reduces the risk of contamination issues. Another benefit of surface texturing is promotion of endothelialization which in turn will reduce the risk for late thrombosis [12, 13].

Drug elution studies are very expensive and are therefore inefficient as a primary means of exploring the effects of laser texturing. To solve this issue, experiments have been conducted to address the feasibility of using surface topography characteristics to determine experimental conditions that will yield a high potential for increased drug adhesion to the stent. The results will be used to manufacture drug eluting stents to be further explored in drug elution studies.

In particular, our experiment explores the effect of the speed of overlapping laser pulses on surface topography. After laser treatment at four different speeds which produced different sizes of overlap, the surfaces were evaluated using a 3D Zygo optical surface

profiler. The profiler records the height after which software was used to measure the following surface characteristics: surface area ratio, surface roughness, volume of lubricant per unit area from the bearing ratio analysis, and mean valley slope. These characteristics, in addition to process time, were then evaluated using the weighted property index method to determine which speed produces surface texture that is likely to improve drug adhesion at a reasonable process time. This method of comparison was chosen because traditional measures of surface topography, such as surface roughness or surface area ratio, are not accurate indicators of adhesion strength without investigating multiple characteristics [8]. In addition, it reduces the effect of multicollinearity on resulting data.

4.2 Methods and Procedures

4.2.1 Laser Processing

Testing began by cutting six coupons approximately 4 mm long from a Nitinol stent shown in Figure 11. The cross section was a square with a side length of 0.35 mm. Each coupon was secured to the same aluminum disk. Coupons were chosen as the sample material for testing to maintain the surface properties and the dimensions of a full sized nitinol stent.

The coupons were processed using a Q-switched Nd:YAG laser with a wavelength of 532 nm, pulse width of 7 ns, and a M^2 beam profile of 1.42. The laser beam was focused to a spot diameter of 0.44 mm using a plano-convex lens with a 25 mm diameter and a 50 mm focal length.

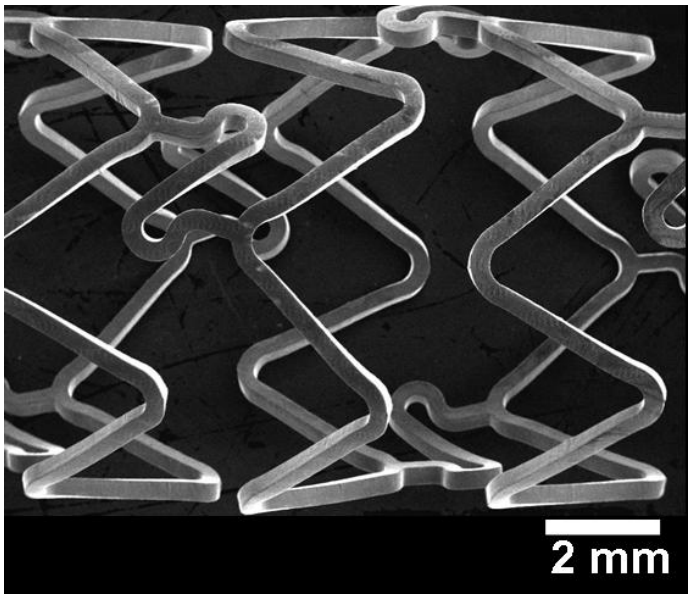

Figure 11: SEM image of an expanded Nitinol stent

One coupon was left untreated to measure the surface topography before laser treatment. Another one of the coupons was used to learn how the laser interacts with Nitinol before exploring overlapping effects. This coupon was held stationary while being treated with two pulses with an average power of 0.08W at a repetition rate of 1 Hz.

The remainder of the coupons were used to investigate overlapping effects. The laser was held stationary while the stage was set in motion. While holding the average power (0.45W) and repetition rate (10 Hz) constant, the speed of the stage was varied to produce different overlaps. The selected speeds were 0.5, 0.75, 1, and 1.25 mm/s. The overlap of parallel paths was 20% based upon the outer diameter of the spot. The direction of motion was set to an approximate angle of 13 degrees with respect to the length of the coupon. This angle was chosen to mimic the treatment to the full sized stent. The stage was programmed to run in a serpentine pattern.

4.2.2 Method of Data Analysis

After the laser treatment, the coupons were imaged using a scanning electron microscope (SEM) for the purpose of visual comparison.

The tool used for quantitative data analysis was a 3D Zygo optical surface profiler. The surface profiler was used to measure the untreated coupon and the coupons that were laser treated while the stage was in motion.

The Zygo optical surface profiler that was used has the ability to stitch the data from multiple areas together using software. This capability yielded a high resolution while allowing data to be gathered over a large area in a short period of time. The 50x objective produced a field of view of 0.14 x 0.11 mm, an optical resolution of 0.52 μm, and a vertical resolution of less than 0.1 nm. In this experiment, a matrix of five rows and fifteen columns with a 32% overlap was determined to be appropriate because it would span a full parallel path created by the laser. This yielded a large area of 1.44 x 0.4 mm which was required to maintain accuracy due to the varying surface topography. The width of 0.4 mm was selected since it was greater than the specifications of the width of the stent to ensure all edge data was included. The length of 1.44 mm was chosen based on the average length of a full parallel path. There was variation due to the inability to precisely place the stent coupons at the same angle with respect to the laser path.

After the data was collected, it was analyzed with the software that accompanies the Zygo optical surface profiler, MetroPro 8.3.4. Before values were recorded, high and low clips were applied. The clips were set in place to remove extreme spikes above the high clip and below the low clip that would alter the accuracy of the data. The high and low clips removed data above and below ±200 nm for the untreated coupon and ±1500 nm for the

treated sections. The trim option reduces errors by trimming the edges of filtered data. This omits extreme edge values that may affect data characteristics.

The first characteristic measured was the surface area ratio. This was chosen to determine the increase in contact area that the drug is able to attach. After the surface area ratio is measured, a high pass filter with a wavelength of 11 µm was applied to measure three more surface characteristics. The filter was necessary to exclude the form and waviness from the analysis. Since the drug does not bond well to the stent without the polymer, the surface topography will be what predominately holds the drug; therefore, it was inspected.

A series of steps were required to select the filter wavelength. First, a high pass Gaussian fast Fourier transform filter was applied. The cutoff wavelength that was automatically selected by the software was used as a starting point. Since it is difficult to see the effects of different cutoff frequencies of a high pass filter on an area, several line segments were chosen to create profiles. The line segments were typically drawn over areas that have a significant variation in height. For example, some lines were drawn over ripple patterns and others were drawn over the highest peaks generated by the laser pulse. Each profile graph was then qualitatively evaluated to determine what cutoff wavelength seemed appropriate. The profile graph showed the original data, waviness, and roughness. The cutoff wavelength selected is one that yielded a relatively smooth waviness curve over the input data for various line segments. The experimenter narrowed the selection for a cutoff wavelength to the range of 7 to 15 µm based on visual observations from the profile graphs of multiple line segments. To reduce error, 11 µm was selected since it is in the middle of the range. This value was applied to each data set to remain consistent. A few line segments were evaluated from each data set to check that 11 µm was appropriate for all of the data.

After the filter was applied, further surface characteristics could be calculated. The second characteristic is the surface roughness. A high surface roughness will indicate that the surface has deeper indentations in which the drug will lie. The third characteristic is the potential volume of lubricant per unit area from the bearing ratio analysis. This volume per unit area will be utilized as an approximation of the drug that remains in the valleys after initial drug release. The fourth characteristic is the mean valley slope which can be thought of as being proportional to the aspect ratio of an indentation. The final factor is the time to process. Since the cost of running a laser will vary by the laser itself, the time required to treat a full sized stent was chosen as the best indicator of cost. When calculating the time required, the length and diameter of the stent were assumed to be 7.0 mm and 31.7 mm respectively.

In order to calculate these characteristics, the data needed to be divided due to the limitations in software capabilities. The filter could not be applied over the entire area due to a lack of computer memory. To solve this problem, the area was divided into two sections cut along the y-direction. Where the sections met, error is expected to occur due to edge calculations. By dividing it only into two sections, the error was limited. A similar issue came about in the limits of the software when calculating mean valley slope. The software had a limit of 10,000 peaks per section. To remedy this issue, the area was divided into eight sections. These sections were also cut in the y-direction. By cutting in the y-direction, each section contained approximately the same area of stent. If the area was cut in the x-direction or cut in a grid pattern, there would be areas with and without data due to positioning of the stent in the area.

Since the data needed to be divided into sections for computations, multiple values were gathered for each of the characteristics desired. Therefore, a predicted value of the overall area was used. The surface area ratio was calculated by dividing the sum of each surface area by the sum of each area then subtracting 1 to yield the increase in surface area. Traditionally, surface roughness is calculated as the average height of data points. To remain consistent, the surface roughness values were averaged. The volume per unit area was calculated as the sum of the volumes of the two areas divided by the sum of the areas. Since the mean valley slope was based off of the number of valleys in the area selected, the overall mean valley slope was calculated by first multiplying each mean valley slope by the number of valleys in that section, and then dividing the sum of those products by the total number of valleys.

After each predicted value of the overall area was calculated, the results were combined using the weighted property index method. This method yields a single number for each speed to decide which is the best choice to further investigate in drug elution trials. As part of this method, weighting factors were assigned to each measured characteristic. To maintain an unbiased decision, pairwise comparison using the data logic method was used to determine the weighting factors.

4.3 Results and Discussion

4.3.1 Characterizing the Three Zones

Figure 12 is an SEM image of the laser treated Nitinol surface. In this test, the sample was hit with two pulses in the same location. It is clear from the image that there are three zones. Zone 1 is the crater formed in the direct center. Zone 2 is the smooth surface outside

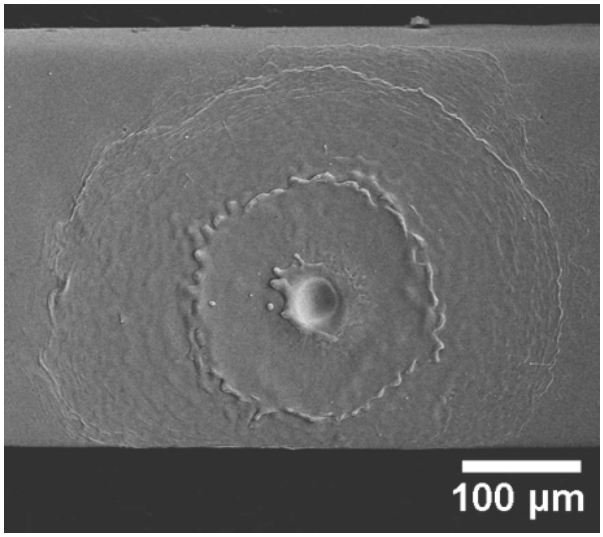

Figure 12: SEM image of two stationary laser pulses

of Zone 1. Zone 3 is identified by the rippled texture outside of Zone 2. The ripple texture in the zone 3 is the most likely feature that will promote adhesion of the drug to the stent; therefore, ideally the goal is to cover the entire stent with the ripple texture.

The zone identifications from Figure 12 are necessary when defining the overlap. The overlap between parallel paths, as stated in the "Methods and Procedures" section, is 20% based on the outer diameter of zone 3. For the overlapping pulses on a single laser path, the overlap produced by the different speeds is 37.5%, 50%, 62.5%, and 75%.

4.3.2 SEM Results

Figure 13a is an image of the stent coupon positioned horizontally. The speed set on this coupon is 1 mm/s. Zone 2 is clearly shown by the overlapping laser pattern that begins in the lower left and follows to the upper right of the image. The purpose for the diagonal was to maintain the conditions that a full sized stent would undergo. Zone 3 is shown more clearly in Figure 13g, a closer image of the area between the overlapping paths of zone 2.

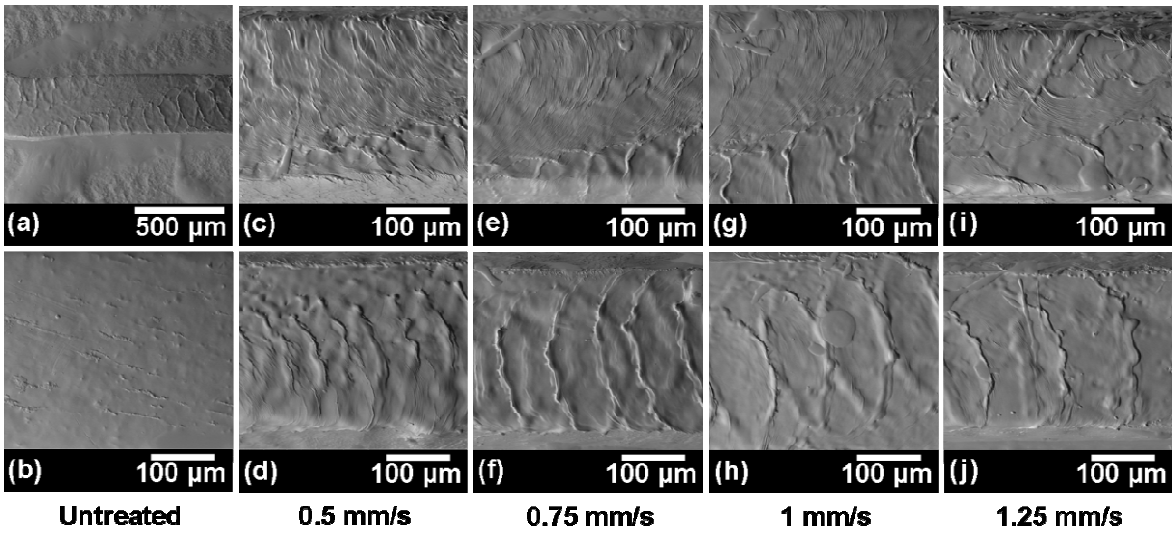

Figure 13: SEM images of a laser treated (a,c-j) and untreated (b) Nitinol stent

Zone 3 contains the ripple texture that is desired. The goal of the experiment is to determine which speed will most likely yield the greatest area containing the ripple texture while considering the time required to laser texture a stent.

Figure 13b shows an example of the surface topography before it is laser treated. It is used as a comparison to the remainder of the images in Figure 13. The untreated surface is very smooth so it is difficult for the drug to bond well to this surface. Laser texturing will provide surface characteristics that will increase the adhesion of the drug to the stent. Since the laser spot diameter is larger than the width of the stent, ripple density will vary because zone 2 will lower ripple density. Figure 13c – j show the two different extremes of ripple density. The top row (Figure 13c, e, g, and i) show areas with significant ripple density. The bottom row (Figure 13d, f, h, and j) show the areas with low ripple density. The columns are organized by the speed of the stage. The second, third, fourth, and fifth columns correspond to 0.5, 0.75, 1, and 1.25 mm/s respectively. Looking at the top row of Figure 13, it is clear that lower speeds yield a greater density of ripples. This is also true for the bottom row

although it is harder to see. For the 0.5 mm/s there is a fair amount of ripple formation, and on the 0.75 and 1 mm/s coupons the ripple texture reduces. The speed of 1.25 mm/s contains the least area of ripple texture. Based upon these images, the speed of 0.5 mm/s is the most likely to yield a large area of ripples. Since it is the least cost effective choice, it will likely not be the option selected for drug trials. Therefore, speeds of 0.75 or 1 mm/s will most likely be the best choices.

4.3.3 Surface Profiler Results

Figure 14a is an example of a two-dimensional plot produced by MetroPro. Height is indicated by the color spectrum. Red displays where the peaks are located, and blue shows the valleys. In this plot, the form was removed using a tool that fits the data to the shape of a cylinder. This plot clearly shows the outer diameter of zone 2 of the parallel laser paths. Zone 3 is difficult to see. As displayed in the image, there are some anomalies shown by a red area surrounded by a blue area. This is caused by a splatter of melted electrical tape that was used to mount the stent to the aluminum disk. This did not appear very frequently; however, it may cause a small error. Another issue that arose is that there are black areas around the high peaks. These are voids of data caused because the slopes that are too high cannot be captured by the surface profiler due to the nature of the device.

Figure 14b and c are a two dimensional plots of the same area as Figure 14a. As discussed before, the entire area could not be processed at once due to the limitations of computer memory. Therefore, the plot was divided into a left half (Figure 14b) and right half (Figure 14c). The difference between the plot from Figure 14a and the plot from Figure 14b and Figure 14c is that the latter is processed by a Gaussian filter with a cutoff wavelength of

11 μm. Most of the area has changed to a green color indicating that the waviness has been removed. Figure 14d is a smaller section with a width that is an eighth of the length of the overall area. This image shows that the surface profiler is able to quantify the ripple formation. A higher resolution was not investigated because the amount of data necessary to cover the same area would be unmanageable to analyze due to the limitations of the computer memory.

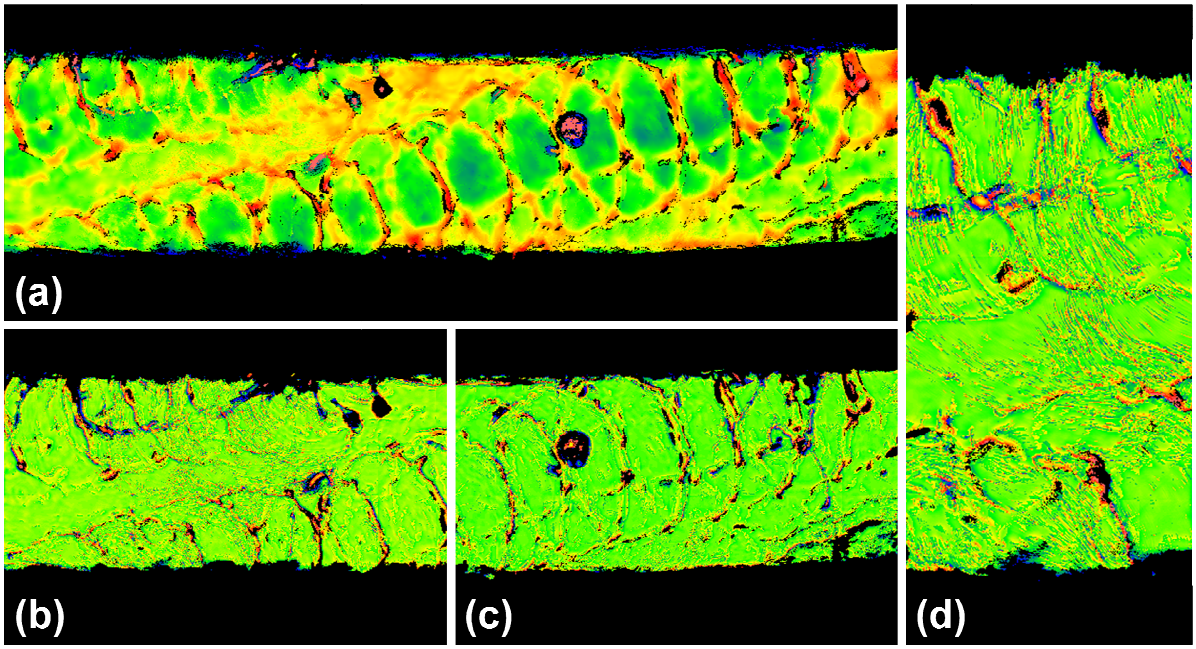

Figure 14: Typical plots from MetroPro of a textured stent coupon where images (b), (c), and (d) are plots after the high pass filter is applied

Since the goal of the experiment is to evaluate which speed will most likely increase ripple formation, each characteristic was plotted against the speed (Figure 15). The data points connected by solid blue lines show the predicted overall value for the characteristic at the corresponding speed. The dashed red line represents the predicted overall value of the untreated stent coupon. This was used as a visual aid to show the improvement due to laser texturing.

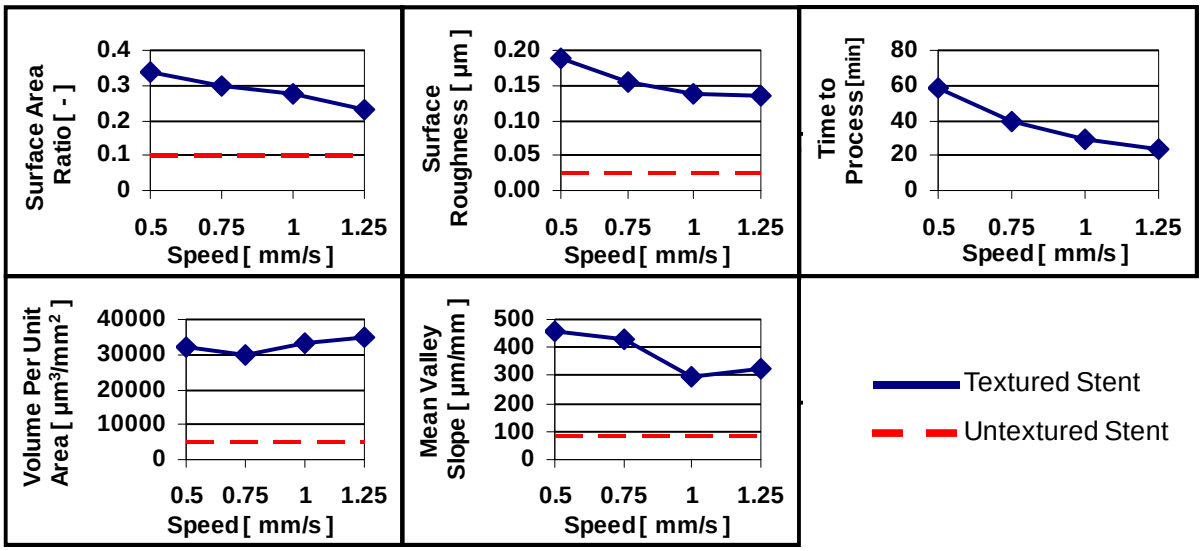

Figure 15: Plots of surface characteristics with respect to speed (the red dashed line represents the overall predicted value of the untreated stent coupon, the blue line shows the overall values of the laser treated coupons for the corresponding speeds)

Figure 15 shows that the surface area ratio, surface roughness, and mean valley slope decrease with increasing speed. For each of those characteristics, the 1.25 mm/s would be the least favorable choice, and 0.5 mm/s would be the best choice. However, in the volume of lubricant per unit area graph the maximum occurs at 1.25 mm/s indicating that 1.25 mm/s is the best choice. The graphs for volume of lubricant per unit area and mean valley slope show some variation from the general trend for speeds 0.75 and 1 mm/s. It is possible that this is caused by variation of the laser power and beam energy distribution. Overall, the data obtained by the surface profiler indicates that the speed of 0.5 mm/s will most likely improve drug adhesion.

After the surface data was analyzed, it was necessary to factor in the cost of the stent through the parameter “time to process”. In order to incorporate time to process into the evaluation, the weighted property index method was chosen as a method of systematically making a decision. The weighting factors assigned to each characteristic were determined by

pairwise comparison using the digital logic method since it provided an unbiased decision. In this approach, each combination of two characteristics was considered. The indicator that would be more important to the overall goal was given a '1' and the other characteristic was given a '0.' The comparison of characteristics and the resulting weighting factors that were selected are shown in Table 2 and Table 3 respectively.

Table 2: Pairwise comparison table

	Surface Area Ratio	Ra Surface Roughness	Volume per Unit Area	Mean Valley Slope	Time to Process
	A	B	C	D	E
A & B	1	0			
A & C	0		1		
A & D	0			1	
A & E	0				1
B & C		1	0		
B & D		0		1	
B & E		0			1
C & D			0	1	
C & E			0		1
D & E				0	1
Sum	1	1	1	3	4

Table 3: Weighting factors of surface characteristics

Characteristic	Weighting Factor
Surface Area Ratio	0.100
Ra Surface Roughness	0.100
Volume per Unit Area	0.100
Mean Valley Slope	0.300
Time to Process	0.400
Total	1.000

Table 2 and Table 3 show that the time to process was more important than the other characteristics which agrees with the logic that it plays a significant role in the decision. Mean valley slope was also very influential and was weighted more heavily because it is a direct measure of the aspect ratio of the valleys. Surface roughness and lubricant volume per unit area had a lower influence since these measurements are not dependent on the aspect ratio of the valleys. In other words, a smoother surface with a low aspect ratio can produce the same surface roughness as that of a rough surface with a high aspect ratio because the calculation is only an average of the absolute height values. Since surface area ratio is a measure related to initial drug release, it was not weighted as significantly. The laser texturing is designed to promote slow release over the long term.

After the weighting factors were determined, each characteristic needs to be scaled by creating β values. These values were determined by multiplying the data value by 100 and dividing by the highest value in the data set for the surface area ratio, surface roughness, lubricant volume per unit area, and mean valley slope because a high value is desired. In the case of the time to process, a low value is desired; therefore, the β value was calculated by multiplying the lowest value in the data set by 100 and dividing by the data value. After calculating the β values for each speed for each characteristic, the performance index was calculated by summing the product of the β value and the weighting factor for each characteristic at a given speed [14]. The performance indexes are shown in Table 4.

Table 4: Performance indexes of speeds

Speed (mm/s)	Performance Index
0.5	75.2
0.75	77.9
1	76.8
1.25	85.5

As shown in Table 4, the speed with the highest performance index is 1.25 mm/s. This single value accounts for surface topography characteristics as well as time to process. Therefore, 1.25 mm/s is the speed that is chosen to be further investigated in drug trials. However, the performance index is subject to change based upon how the characteristics are weighted. For instance, if a manufacturer has performed a market study showing that the benefits of the slower speed would outweigh the time to process, the weighting factor for the time to process would be lowered. In this case the trade off would be sacrificing an increase in cost for a higher quality product. If the weighting factor for the time to process was set to a different value, it would be eliminated from the pairwise comparison table, and then the rest of the characteristics will be adjusted accordingly. For example, if the weighting factor of the time to process was set to 0.15, then the weighting factors for surface area ratio, surface roughness, lubricant volume per unit area, and mean valley slope would become 0.14, 0.14, 0.14, and 0.425 respectively. The performance indexes would become 89.8, 85.3, 75.4, and 79.5 for the speeds 0.5, 0.75, 1, and 1.25 respectively. This indicates that speeds slower than 0.5 mm/s would be worth investigating to determine which speed will yield the best texture.

4.4 Conclusion

Five stent coupons were processed using a Q-switched Nd:YAG laser with a wavelength of 532 nm, pulse width of 7 ns, and a spot diameter of 0.44 mm. One coupon was not laser treated, and the other four coupons were treated while the coupons were in motion at 0.5, 0.75, 1, and 1.25 mm/s. The coupons were evaluated based upon surface area ratio, surface roughness, lubricant volume per unit area, mean valley slope, and the time to process. The weighted property index method yielded that 1.25 mm/s was the best choice of speed.

This produced a 129% increase in surface area ratio, 409% increase in surface roughness, 618% increase in volume per unit area, and 287% increase in mean valley slope.

Since there is variation in the samples, the experiment should be repeated with multiple samples at each speed, and the mean for each speed should be used for calculating the performance index. The method of utilizing the Zygo surface profilometer and MetroPro software in addition to performing calculations on the data gathered yielded a systematic but efficient method of evaluating which speed choice would have the greatest potential for success in drug trials.

4.6 Acknowledgments

We like to acknowledge the support provided by National Science Foundation under the grant IIP-0944979.

4.7 References

1. Hara, H., Nakamura, M., Palmaz, J., and Schwartz, R., 2006, “Role of Stent Design and Coatings on Restenosis and Thrombosis,” Advanced Drug Delivery Reviews, **58**(3). pp. 377–386.
2. Heldman, A., Cheng, L., Jenkins, G.M., Heller, P., Kim, D.-W., Ware, M., Nater, C., Hruban, R., Rezai, B., Abella, B., Bunge, K., Kinsella, J., Sollot, S., Lakatta, E., Brinker, J., Hunter, W., and Froehlich, J., 2001, “Paclitaxel Stent Coating Inhibits Neointimal Hyperplasia at 4 Weeks in a Porcine Model of Coronary Restenosis,” Circulation, **103**(18), pp. 2289–2295.
3. Acharya, G., and Park, K., 2006, “Mechanisms of Controlled Drug Release from Drug-eluting Stents,” Advanced Drug Delivery Reviews, **58**(3), pp. 387–401.

4. Yang, S., Man, H., Xing, W., and Zheng, X., 2009, "Adhesion Strength of Plasma-sprayed Hydroxyapatite Coatings on Laser Gas-nitrided Pure Titanium," Surface & Coatings Technology, **203**(20–21), pp. 3116–3122.
5. Bahbou, M., Nylen, P., and Wigren, J., 2004, "Effect of Grit Blasting and Spraying Angle on the Adhesion Strength of a Plasma-sprayed Coating," Journal of Thermal Spray Technology, **13**(4), pp. 508–514.
6. Varacalle, D., Guillen, D., Deason, D., Rhodaberger, W., and Sampson, E., 2009, "Effect of Grit-Blasting on Substrate Roughness and Coating Adhesion," Journal of Thermal Spray Technology, **15**(3), pp. 348–355.
7. Asl, S.K., and Sohi, M.H., 2010, "Effect of grit-blasting parameters on the surface roughness and adhesion strength of sprayed coating," Surface and Interface Analysis, **42**(6–7), pp. 551–554.
8. Lee, C., Rasiah, I., Chong, C., and Gopalakrishnan, R., 1997, "The Role of Surface Morphology on Interfacial Adhesion in IC Packaging," Proceedings of the 1997 1st Electronic Packaging Technology Conference, pp. 201–207.
9. Mohammadi, Z., Ziaei-Moayyed, A.A., and Mesgar, A.S.M., 2007, "Grit blasting of Ti-6Al-4V alloy: Optimization and its Effect on Adhesion Strength of Plasma-sprayed Hydroxyapatite Coatings," Journal of Materials Processing Technology, **194**(1–3), pp. 15–23.
10. Man, H., Chiu, K., and Guo, X., 2010, "Laser Surface Micro-drilling and Texturing of Metals for Improvement of Adhesion Joint Strength," Applied Surface Science, **256**(10), pp. 3166–3169.

11. Mehilli, J., Kastrati, A., Wessely, R., Dibra, A., Hausleiter, J., Jaschke, B., Dirschinger, J., and Schömig, A., 2006, "Randomized Trial of a Nonpolymer-Based Rapamycin-Eluting Stent Versus a Polymer-Based Paclitaxel-Eluting Stent for the Reduction of Late Lumen Loss," Circulation, **113**(2), pp. 273–279.
12. Dibra, A., Kastrati, A., Mehilli, J., Pache, J., Oepen, R., Dirschinger, J., and Schömig, A., 2005, "Influence of Stent Surface Topography on the Outcomes of Patients Undergoing Coronary Stenting: A Randomized Double-Blind Controlled Trial," Catheterization and Cardiovascular Interventions, **65**(3), pp. 374–380.
13. Loya, M., Brammer, K., Choi, C., Chen, L.-H., and Jin, S., 2010, "Plasma-induced Nanopillars on Bare Metal Coronary Stent Surface for Enhanced Endothelialization," Acta Biomaterialia, **6**(12), pp. 4589–4595.
14. Dieter, G., and Schmidt, L., 2009, "Engineering Design," McGraw-Hill Higher Education, 4th ed., Boston, MA.

CHAPTER 5. GENERAL CONCLUSIONS

Though drug eluting stents have significant advances in reducing restenosis over bare metal stents, further research is required to decrease the likelihood of late stent thrombosis. The experiment reported in chapter 3 addresses the concept of using laser texturing as a potential solution to eliminate the hypersensitivity caused by polymers on DES which increase the potential for LST. Chapter 4 introduced a method of sample comparison in order to predict experimental conditions that would promote drug adhesion to the stent surface thus reducing the number of expensive drug elution trials.

In the first experiment, laser induced periodic surface structures were generated on Nitinol stent surfaces using a Q-switched Nd:YAG laser with a wavelength of 532 nm and pulse width of 7 ns. Laser texturing parameters were chosen to maximize ripple formation while minimizing processing time allowing for commercial implementation. Ripple patterns were shown to have a period ranging between 400 nm and 1000 nm suggesting that the ripple structures can provide adequate surface texture to aid in drug adhesion. Surface profiler results demonstrated that laser texturing significantly improves surface topography over bare metal stents. With a 488% increase in volume per unit area, laser texturing dramatically increases the volume of drug that can be held in the valleys of the stent surface. In addition, the mean valley slope was improved by 420%, indicating that the aspect ratio of the valleys is significantly higher which equates to a higher resistance to erosion from blood flow. Because surface analysis demonstrated that laser texturing has a great potential to promote drug adherence, it was necessary to test the feasibly in a drug elution study.

The preliminary drug elution study proved that nanosecond laser textured stents warrant further investigation. In the comparison of cumulative release rates of the four stents,

the biodegradable polymer did not increase drug adherence to the stent nor did it slow the drug release rate. In contrast, laser texturing improved drug adherence and demonstrated a steady release rate. The rate of drug release is significantly slower in laser textured stents indicating that the drug has a potential to be released over a longer period of time than traditional drug eluting stents. Laser texturing parameters can be controlled to allow for a faster or slower release to reach the desired range of drug concentration. Laser texturing offers steadier release rates and better drug adhesion than the biodegradable polymer, which is an alternative to current nondegradable polymers. This suggests that laser texturing has the potential to eliminate the need for polymers in drug eluting stents.

The second experiment demonstrates that the Zygo surface profilometer and MetroPro software are tools that when combined with the weighted property index method will yield an efficient method of evaluating experimental samples to determine what experimental conditions will promote drug adherence to a stent surface. The surface profiler proved to efficiently record height measurements over a large area in fifteen minutes per sample with reasonable spatial resolution. Alternative tools that offer higher resolutions, such as an atomic force microscope, do not offer measurements over a large area.

The weighted property index method proved that 1.25 mm/s is the best choice of speed of the four selected based on surface area ratio, surface roughness, lubricant volume per unit area, mean valley slope, and the time to process. It is important to note that the manufacturer of the stent may choose to make a trade off choosing a higher quality of stent instead of a lower cost stent which may lead to a slower scan velocity. Now that this method is proved to be feasible, it is necessary to repeat the experiment to have a better understanding of the limits of variation.

CHAPTER 6. FUTURE WORK

Feasibility experiments were conducted proving that laser texturing of stent surfaces will promote adherence of a drug to the surface and also that the Zygo optical surface profiler provided an efficient method of analyzing textured surfaces to help determine what experimental conditions will yield the best texture to promote drug adherence. It is important to understand the variability of laser texturing by repeating the experiment performed in chapter 4 using the same speeds with multiple samples. This should be performed by separating the rings of four stents and laser texturing one ring from each stent at one speed. This process should be repeated for three additional speeds. Once each ring is textured, it should be cut into coupons, mounted to a flat surface, and measured using the surface profiler. The surface characteristics should be analyzed for variability. In addition to comparing different speeds, power, repetition rate, and intensity profiles should also be investigated. Once a conclusion is made as to the optimum experimental conditions, elution tests should be conducted to determine how the solution performs at reducing the likelihood of LST. In future elution studies, stent expansion should occur after drug coating to determine the effects of stent expansion on the drug.

The following discussion will expand on the potential of using different intensity profiles to more efficiently produce LIPSS. A change in the intensity profile of a laser through the use of optics will yield different surface textures on the stent that are specific to each optic. Surface analysis would be conducted to evaluate the different intensity profiles to determine which profile will efficiently yield surface topography that has the greatest potential to improve drug retention on the stent. The optics that are desired for testing include

a spherical plano-convex lens, cylindrical plano-convex lens, a Gaussian-to-TopHat converter (aspheric lens pair), and an axicon lens focused with a spherical plano-convex lens.

As previously explained in chapter 3, the formation of ripples occurs when the laser intensity heats the surface to a temperature near the melting threshold. We hypothesize that the ideal solution would be one that could create a consistent intensity over the entire area to heat it to near the melting threshold. In order to utilize this knowledge, we must modify the intensity profile using different optics to maximize the ripple formation. The best solution will be based both on maximizing ripple formation while minimizing time required to laser texture a stent.

Predictions of the intensity profiles must be compared to determine the potential surface patterns (Figure 16). Each relative intensity profile is generated based on maintaining consistent volumes under the three dimensional intensity profiles. Relative intensities are used here with the expectation that the power can be adjusted during testing to yield the greatest ripple coverage.

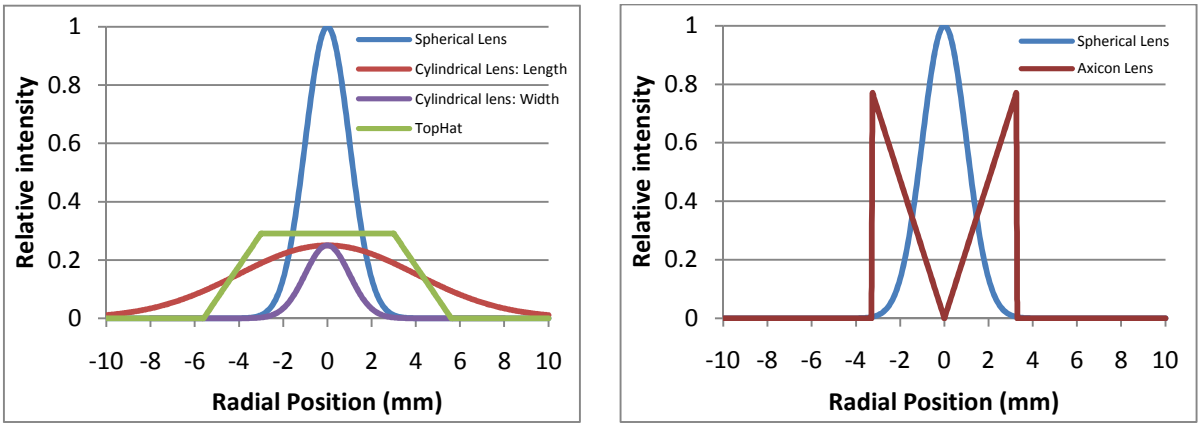

Figure 16: Relative intensity profile of a spherical lens, cylindrical lens, Gaussian-to-TopHat converter, and axicon lens paired with a spherical lens

The axicon lens paired with a spherical lens is desired for testing because of its unique intensity profile that orients the highest intensity to be located on the outer ring and the lowest intensity to be in the center. Figure 17 illustrates how the intensity can be reversed depending on the positioning of the sample. Further research is required to determine the exact shape of the profile.

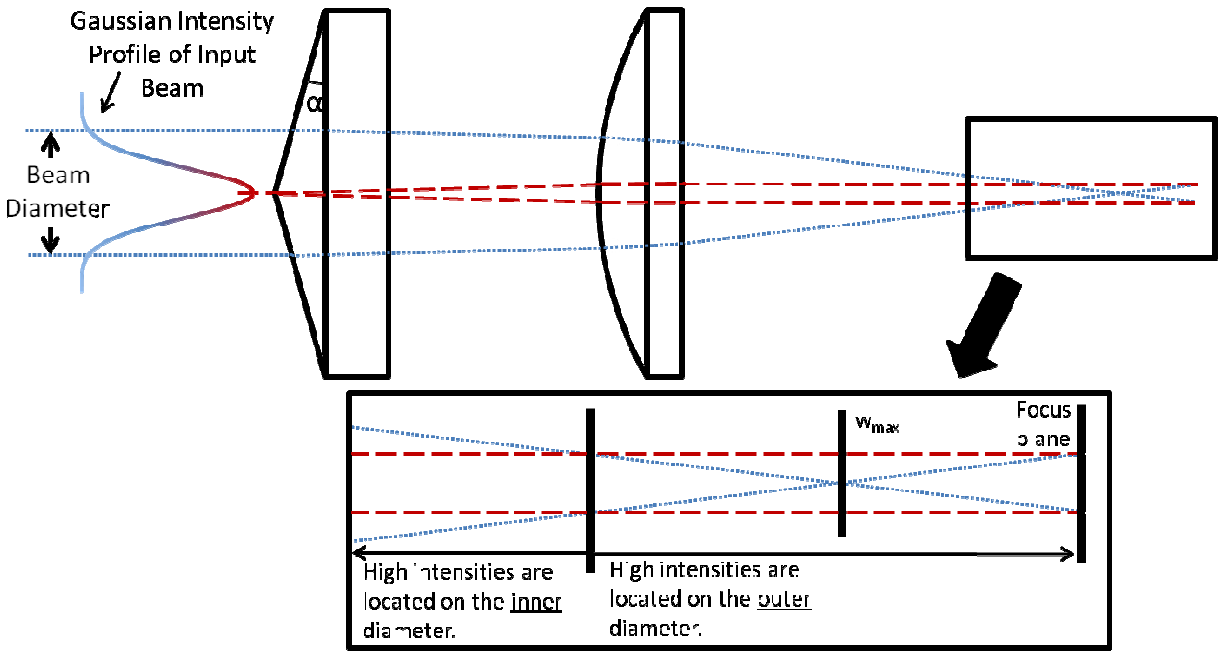

Figure 17: Illustration of how the Gaussian intensity profile of an input beam can be reversed in a certain region

As shown in Table 5, the spherical lens is least desirable. The next choice is the cylindrical lens; it can significantly reduce process time (because the length is much longer) while producing good ripple density per pulse. The second best choice is the aspheric lens pair (tophat). Though the consistent ripple density enables a lower process time due to lower overlap, the precision alignment and beam quality requirements are concerning. The axicon and spherical lens pair is the most desirable because the ripple density per pulse is excellent in addition to a significantly reduced process time.

Table 5: Lens characteristics

	Expected Ripple Density/Pulse Scale (1-4)	Time to Process (min)	Length		Width	
			Size (mm)	Overlap (%)	Size (mm)	Overlap (%)
Spherical Lens	Poor (1)	60	0.44	10	0.44	40
Cylindrical Lens	Good (3)	28	1.65	61	0.13	60
TopHat (Aspheric Lens Pair)	Excellent (4)	6	0.66	10	0.66	30
Axicon and Spherical Lens Pair	Excellent (4)	17	0.80	10	0.80	70

The time to process in Table 5 is based upon texturing a full sized stent where the length and diameter of the stent were assumed to be 7.0 mm and 31.7 mm respectively. Given the spot size as described in Table 5 by length and width, the time to process is calculated based upon the overlap and a constant repetition rate of 10 Hz. The spherical lens was based upon the speed that was determined to yield the greatest ripple density per pulse. The size of the cylindrical lens was based off of the length and width of a pulse created with the same Q-switched Nd:YAG laser used throughout this study. The size of the TopHat profile is based upon a 0.66 x 0.66 mm Gaussian-to-TopHat converter that can be purchased from LIMO Lissotschenko Microoptic. Lastly, the axicon and spherical lens pair size is based upon calculations performed in SolidWorks that determined the path of light as it was refracted through the axicon and spherical lens pair.